Buckling of Internally-Pressurized Spiral-Welded Steel Pipes under Bending

Buckling of Internally-Pressurized Spiral-Welded Steel Pipes under Bending

C. I. Papadaki [a], S. A. Karamanos [a, b, 1], G. Chatzopoulou [a] and G. C. Sarvanis [a]

[a] Department of Mechanical Engineering, University of Thessaly, Volos, Greece

[b] Institute of Infrastructure and Environment, School of Engineering, The University of Edinburgh, Scotland, UK

ABSTRACT

The mechanical behaviour of spiral-welded large-diameter steel pipes is simulated, with the purpose of defining their bending deformation capacity against local buckling. The steel pipes are candidates for hydrocarbon onshore pipeline applications with diameter-to-thickness ratio D/t equal to 53 and 69, and are subjected to longitudinal bending under internal pressure levels ranging from zero to 75% of the nominal yield pressure. Initial geometric imperfections are considered in the form of short-wave axial wrinkles and girth weld misalignment, whereas residual stresses are taken into account as computed from a special-purpose finite element simulation of the spiral bending process, which also accounts for both de-coiling process and hydrotesting. The sensitivity of critical bending curvature on the level of internal pressure is examined, the value of buckling wave length is discussed and the effects of hydrotesting after spiral forming on structural performance are also investigated. Finally, the value of critical bending curvature is compared with analytical and empirical equations, widely used in pipeline design applications. The results of the present study determine the main parameters affecting the buckling deformation capacity of large-diameter spiral welded pipes in a strain-based design framework, and indicate that these pipes can be used in demanding pipeline applications, such as in geohazard areas.

INTRODUCTION

Large-diameter steel pipes, produced through the spiral-welding manufacturing process, are extensively used in large-diameter onshore pipelines for the transmission of energy (hydrocarbon) or water resources. In geohazard areas, ground movements caused by tectonic fault movement, ground subsidence, landslides or liquefaction-induced lateral spreading, can cause severe bending of the

[1] Corresponding author. Email: skara@mie.uth.gr

pressurized pipeline [1]. Severe bending may also be developed due to permafrost subsidence in arctic regions. In those geohazard areas, in addition to pipeline design against pressure containment, the pipeline should also be designed against pressurized bending conditions to sustain the expected ground-induced deformations without loss of containment.

Bending and buckling of thin elastic circular cylinders in the presence of internal pressure has been recognized as an important issue for the safe design of aerospace shell structures, and consequently has received quite some attention in the past [2] [3] [4]. The main conclusion from these works is that the presence of internal pressure has a significant effect on the structural response of the bent cylinder, reducing prebuckling deformation, thus increasing the bending capacity of the thin-walled elastic cylinder. Similar conclusions have been reported by a relatively recent publication by Mathon and Limam [5], based on a series of pressurized bending tests on short cylinders. The stabilizing role of internal pressure on the structural response of thin-walled metal cylindrical shells that buckle in the elastic range of the metal material has also been noticed in several numerical works on the subject [4] [6] [7]. The reader is also referred to the paper by Houliara and Karamanos [8] for a finite element analysis and an extensive discussion of the structural response and buckling of elongated pressurized elastic cylinders, with emphasis on the effects of pressure on critical moment, curvature and the corresponding buckling wave length.

On the other hand, the assumption of elastic material behaviour adopted in the above numerical works may not be valid for bending analysis of steel pipes and tubes employed in offshore structures and pipeline applications. Those cylindrical members are relatively thick-walled, with diameter-to-thickness ratio D/t less than 100, and exhibit inelastic deformation before the occurrence of local buckling. Furthermore, for lower values of D/t ratio, steel pipes may show a substantial deformation reserve beyond initial wrinkling, as noticed in several experimental works [9] [10]. Notable publications with experimental testing results on small-diameter tubes subjected to bending have been reported by Wilhoit and Merwin [11], Tugcu and Schroeder [12], Reddy [13] and Kyriakides and Ju [14]. While the bending response of thin-walled cylinders is characterized by a sudden failure due to local buckling formation, the structural instability of relatively thick-walled cylinders that buckle inelastically occurs more gradually, following a sequence of events associated with pipe wall wrinkling, as described extensively in [14] and in its companion paper [15]. Moreover, a simulation of the structural behaviour of fabricated tubes, has been reported by Karamanos and Tassoulas [16], using an in-house finite element technique.

The presence of internal pressure stabilizes pipe cross-section with respect to local buckling, and results in an increase of structural load capacity of the pipe (axial or bending). The contribution of pressure on the uniform axial load capacity of relatively thick metal tubular specimens has been shown in several recent tests, supported by analytical calculations [17] [18]. For the case of pressurized steel pipes subjected to bending, tests have been reported by Gresnigt [19], motivated by the need for safeguarding gas pipeline integrity in settlement soils. The pipes tested in [19] were reduced-scale size pipes (122-mm and 152-mm-diameter), as well as large-scale size pipes (609-mm-diameter), fabricated from hot-rolled plates. In that publication, analytical models were also developed to support the test results. In a subsequent publication, Van Foeken and Gresnigt [20] have investigated the response of unpressurized and pressurized 160-mm-diameter seamless X42 steel pipes with diameter-to-thickness ratio equal to 100. In those tests, the stabilizing effect of internal pressure has been demonstrated; internally-pressurized specimens at 15% of yield pressure have been capable of sustaining 33% more bending deformation prior to local buckling failure than the non-pressurized pipes. Numerous experiments on large-diameter pressurized pipes have been performed during the last 25 years at the University of Alberta, Canada [21] [22] [23] [24]. The results from those tests have been summarized in [25], and design equations were reported for the compressive capacity of pressurized steel pipelines, which have been adopted by relevant design guidelines [26].

Suzuki *et al.* [27] reported two full-scale tests on 30-inch-diameter X80 steel pipes with D/t ratio equal to 49, pressurized up to 120 bar (equal to 53% of yield pressure). The pipes were bent to a significant curvature before the onset of buckling in the form of an outward local bulge, and the corresponding ultimate bending curvature was quite higher than the curvature at which pipe wall wrinkling was first observed. More recently, combined experimental/numerical work on pressurized bending of small-scale pipes has been recently reported by Limam *et al.* [28]. The specimens were 1½-inch-diameter stainless steel seamless pipes, with D/t ratio equal to 52 and were bent up to 75% of yield pressure. It was observed that for high levels of internal pressure, the pipe specimens were capable of sustaining a significant value of bending curvature, before structural failure occurred due to local buckling. The shape of the buckle in pressurized pipes depends on the level of pressure, as shown in the numerical results of Figure 1, reported in [29], simulating the tests of Limam *et al.* [28]; for zero pressure, the buckle shape has the form of an inward kink, whereas for higher pressure levels the buckle shape is form of an outward bulging pattern.

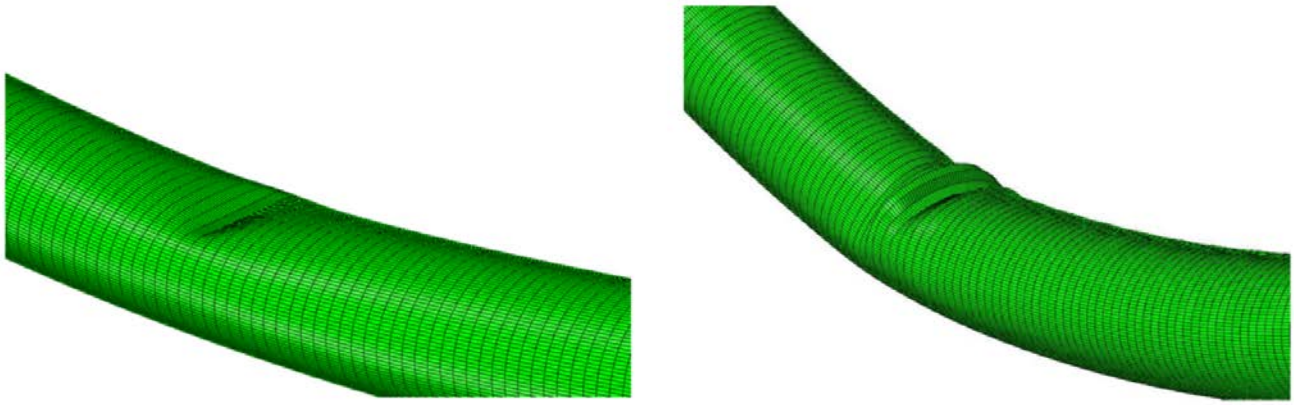

Figure 1: Buckling shapes obtained numerically [29], simulating the bending tests on small-diameter stainless-steel pipes reported in [28] under: (a) zero pressure and (b) pressure equal to 40.3% of yield pressure; the depicted numerical shapes compare very well with the corresponding experimental observations, as reported in [28].

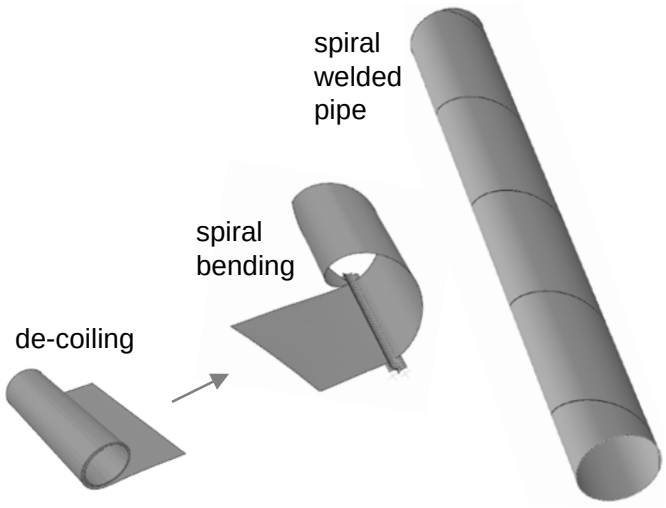

Figure 2: Schematic representation of spiral-welded pipe manufacturing.

Nowadays, there exists an increasing interest in using spiral-welded steel pipes, also referred to as "helical-welded pipes", and denoted as "HSAW pipes", for large-diameter high-pressure hydrocarbon transmission onshore pipelines. However, the use of such pipes in demanding pipeline applications, such as geohazard areas, has been generally limited. On the other hand, the recent advancements in the metallurgical and manufacturing process of spiral-welded pipes, are quite promising for their use in such demanding pipeline applications.

~~In the above framework~~ Line pipe manufacturing may have a significant effect on the structural performance of steel pipelines requires thorough investigation. Experimental results on four 30-inch-

diameter spiral-welded pipes have been reported by Zimmerman *et al*. [31], subjected to various combinations of internal pressure, axial force and bending. The pipe specimens were fabricated using two material grades (X70 and X80) and their thickness corresponded to two D/t ratios (82 and 48). It was concluded that the presence of the spiral weld was in no way detrimental to the pipe structural performance. Tests on two 48-inch-diameter steel pipes, one UOE pipe and one spiral-welded pipe, have been reported in [32] and [33]. The results indicated that the spiral-welded pipe was quite satisfactory, and suitable for use in areas with ground-induced actions. More recently, four experiments have been performed by Zimmerman *et al*. [34] on 36-inch-diameter spiral-welded pipe specimens; the main conclusion was that the measured bending deformation capacity has been larger than the one predicted by available design equations. In that work, material testing has also been conducted, indicating a substantial anisotropy of the steel material due to the manufacturing process.

An extensive experimental study on the bending behaviour of non-pressurized spiral welded tubes, employed in combiwall structural systems, have been reported in [35] and [36]. More specifically, Reinke *et al*. [35] performed eight (8) bending tests on 32-inch and 34-inch-diameter spiral-welded tubes, whereas Van Es *et al*. [36] conducted thirteen (13) bending tests on 42-inch-diameter spiral-welded tubes with diameter to thickness ratio D/t ranging from 65 and 120. These experiments have been supported by extensive numerical simulations, which focused on the effects of initial imperfections and material properties on the structural performance of non-pressurized spiral-welded tubes [37]. Peters *et al*. [38], also motivated from combiwall applications, have performed twenty four (24) bending tests on 20-inch and 24-inch-diameter spiral-welded tubes with D/t equal to 102, filled with sand; the presence of sand provided a restraint against cross-sectional ovalization, and had a beneficial effect on the bending capacity of the tubes.

It should be noticed though that despite the recent advancements in spiral-welding production process that increase the quality of manufacturing and reduce the fabrication cost, as well as the performance of several full-scale experiments, spiral-welded pipes have limited use in demanding pipeline applications and, in particular, in geohazard areas. This is attributed to the lack of sufficient fundamental knowledge on their tensile and compressive strain capacity. The present paper is motivated by the need for establishing safe bending deformation limits for extending the applicability range of spiral-welded pipes in geohazard areas, and constitutes part of a research project, with acronym SBD-SPIPE, sponsored by the European Commission. The project investigated on the use of large-diameter spiral-welded pipes in demanding pipeline applications [39], sponsored by the European Commission through the Research

Fund for Coal and Steel (RFCS). In particular, the work described in the present paper is aimed at determining bending deformation limits for pressurized bending of such pipes, and evaluate the relevant design provisions in existing standards and guidelines. The bending response of two large-diameter spiral-welded pipes is analyzed using finite element simulation tools. The pipes are pressurized up to 75% of the nominal yield pressure and have diameter-to-thickness ratio D/t equal to 53.5 and 69.7 respectively, and are both candidates for use in gas transmission pipeline applications. The effects of spiral cold bending manufacturing process on the bending response are taken into account using a finite element simulation of de-coiling, straightening and spiral bending of a steel coil strip of appropriate thickness and width, as described in detail elsewhere [40], and the residual stresses are used as initial stresses in the pressurized bending model. The numerical model is also employed for the prediction of the structural response of a 36-inch-diameter internally-pressurized pipe, conducted in the framework of the SBD-SPIPE project [39]. Sensitivity of the results on the level of internal pressure, wrinkling imperfection amplitude and girth weld misalignment is also investigated. The results are compared with empirical equations for buckling strain under pressurized bending conditions, widely used in strain-based design procedure. Finally, the value of the corresponding buckling wavelength and the development of local stresses and strain at the buckled area, beyond the buckling stage are also examined and discussed in detail.

NUMERICAL MODEL DESCRIPTION

A numerical model has been developed in ABAQUS/Standard for simulating the bending response of internally pressurized pipes. First, a large-scale experiment on pressurized spiral-welded pipe specimen reported in [39] is simulated. Subsequently, using the model, an extensive numerical study is performed, to be presented in a subsequent section of the paper. The pipes are modeled with four-node reduced integration shell finite elements (S4R), which allow for shear deformation and thickness variation, and are suitable for thin and thick shell analysis. A “rectangular” mesh of shell elements is employed~~, as shown in Figure 3a~~. A relatively dense mesh of shell elements is used, with size of each element equal to about 0.4% of the pipe diameter, so that the wrinkling pattern of local buckling is described accurately. Comparison of results from a “rectangular” mesh with a “spiral” mesh reported in [37], indicated negligible differences in the bending-moment diagram.

The pipe is considered initially imperfect, with a wavy-type (wrinkling) geometric imperfection, in the form of the first buckling mode, obtained through a standard eigenvalue analysis of the pipe under consideration, subjected to pure bending loading performed in ABAQUS. This is a short-wave wrinkling

pattern on the all along compression side of the bent tube, as shown in Figure 3a and Figure 3b. The maximum initial wrinkling amplitude w_0 (imperfection amplitude) is the maximum deviation of the wrinkled shell surface from the perfect cylinder (Figure 3c) and the half wavelength defined as Figure 3c shown, expressed as a fraction of pipe thickness w_0/t. For the particular case of a pipe containing a girth weld, this weld is considered in the middle of the pipe segment under consideration. In that case, a small misalignment between the two adjacent parts (referred to as "girth weld high-low misalignment", or simply "hi/lo") has also been taken into account, imposing an offset in the transverse direction of one pipe part with respect to the other.

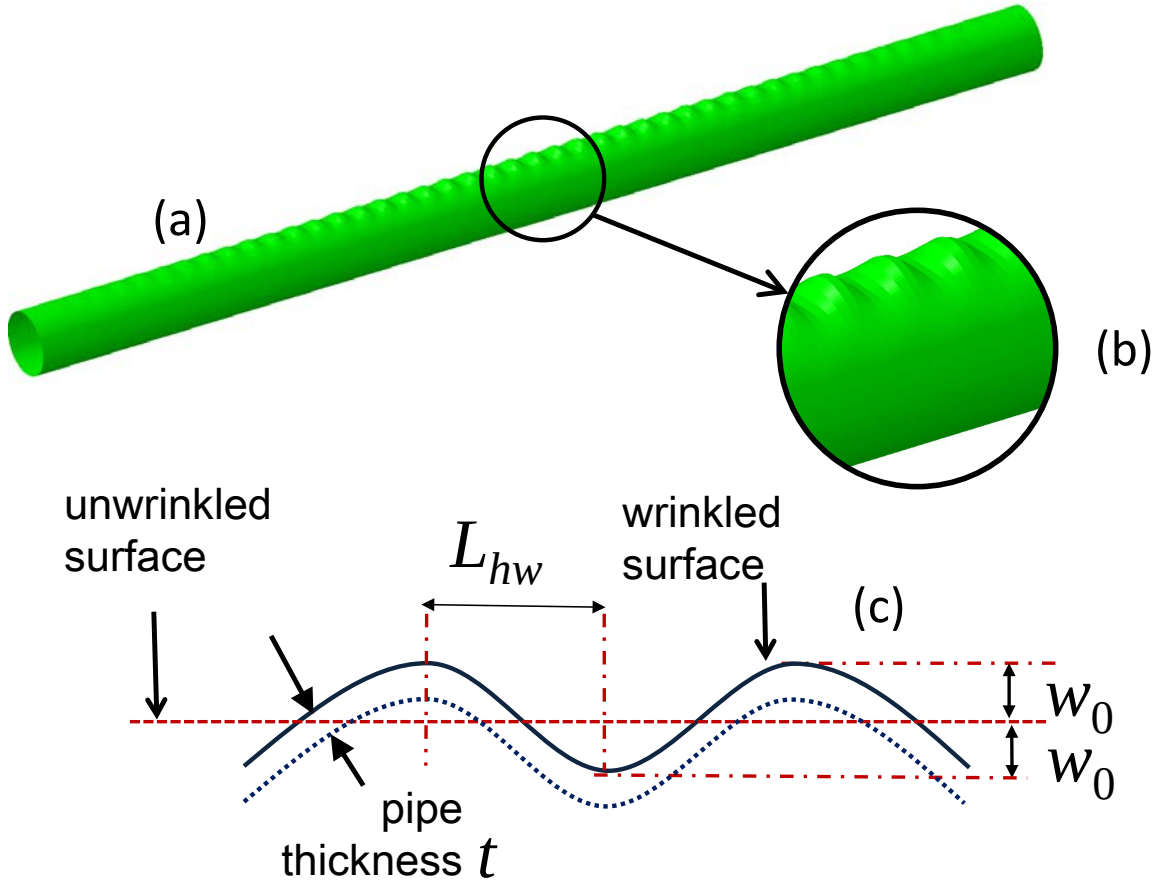

Figure 3: Initial wrinkling geometric imperfection.

Four reference nodes have also been introduced in the finite element model to represent the characteristic locations of the four-point bending test set-up described in [39], to be simulated in the next section of the present paper. The general geometry of the experimental set-up, and the corresponding support and loading conditions are shown in Figure 4. Two reference points refer to the end supports, namely points (A) and (D), and the other two reference points (B) and (C) to the locations where forces

are applied, simulating accurately the test conditions. The translational degrees of freedom at each reference point have been coupled with the translational degrees of freedom of the corresponding cross-section nodes through the application of kinematic conditions. Bending loading is applied through the two vertical upward forces at the inner reference points (B) and (C), leading to a four-point bending loading pattern. A displacement-control analysis procedure is employed to trace the load-displacement path, accounting for buckling and post-buckling, capable at describing accurately "snap-through" instabilities.

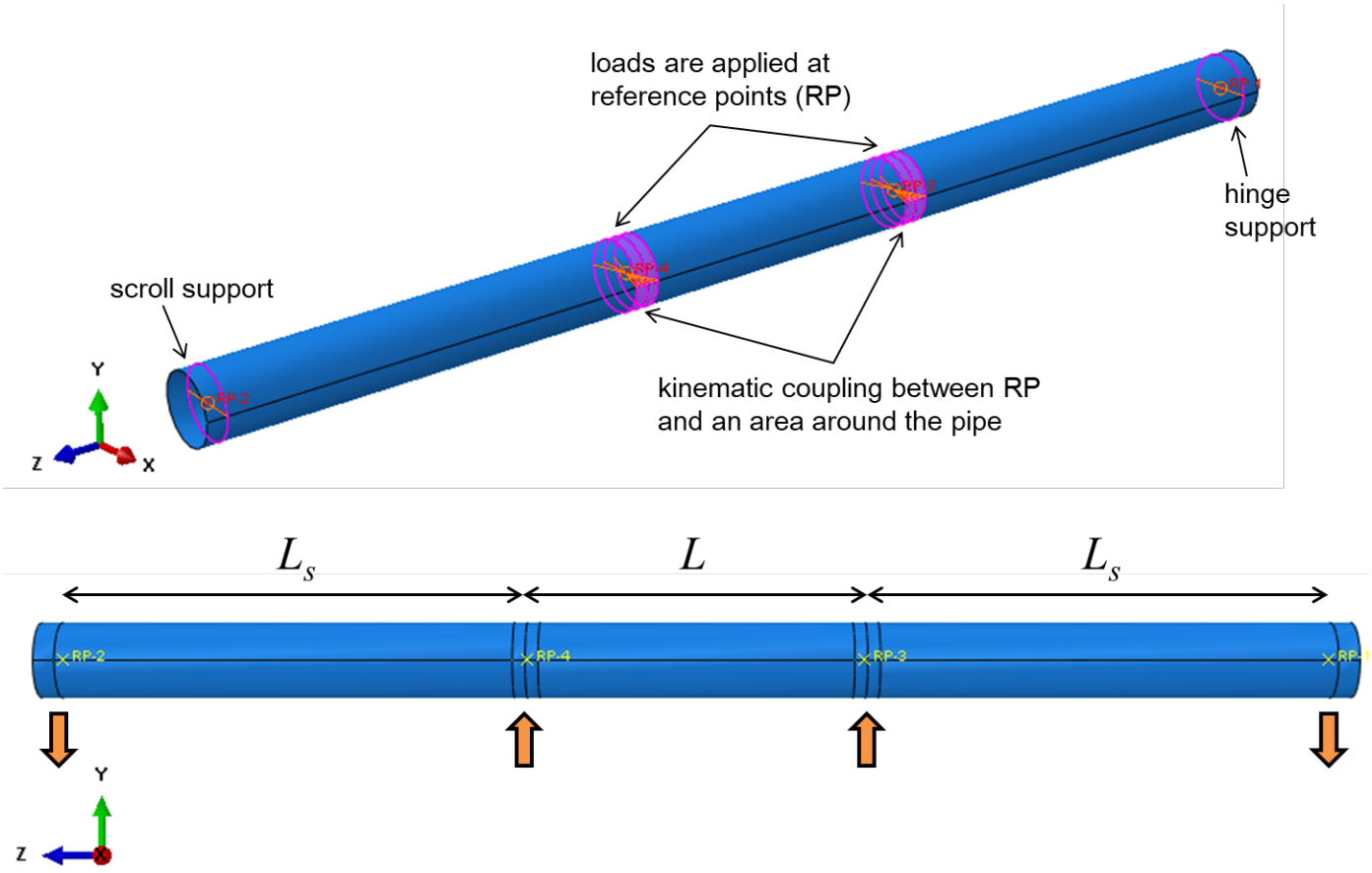

Figure 4: Four-point bending loading pattern for pipe bending.

To account for material inelastic behavior, a von Mises plasticity model with isotropic hardening is considered. Furthermore, residual stresses are inserted in the finite element model as initial stresses before the application of bending loading, as calculated from a detailed simulation of the cold bending mechanism (including de-coiling process), which is presented in detail elsewhere [42], and is described briefly in the Appendix. Finally, before the application of internal pressure and bending loading, a hydrotesting loading step is performed corresponding to hydrotesting of the spiral-welded pipe in the pipe mill. In the present study, hydrotesting is considered equal to the nominal yield pressure of the pipe ($p_0 = 2\sigma_Y t/D$).

COMPARISON WITH EXPERIMENTAL TESTING RESULTS

The numerical tools described above, are employed to predict the structural response of a 36-inch-diameter spiral-welded pipe tested in bending by Salzgitter Mannesmann Forschung GmbH (SZMF) [39]. This full-scale test has been conducted in the course of European research program SBD-SPIPE. The pipe specimen is a 15.5m-long, 36-inch-diameter spiral-welded pipe, with nominal thickness 17.1mm, X70 steel material, and has been manufactured by SZMF [39]. Details thickness measurements have indicated that the average thickness of the pipe is equal to 17.5 mm. The internal pressure of the pipe specimen was equal to 13.5 MPa (135 bar), which is 72% of the yield pressure. The angle of the spiral is equal to 31.5 degrees, the width of the coil is 1501 mm, and the uniaxial stress-strain curve of pipe steel material is shown in Figure 5.

In the following, the values of bending moment and curvature are normalized by the fully-plastic moment $(M_P = \sigma_Y D^2 t)$ and the curvature parameter $\kappa_1 = t/D^2$ respectively, whereas the internal pressure is normalized by the yield pressure ($p_0 = 2\sigma_Y t/D$). In all those expressions, D is the mean pipe diameter.

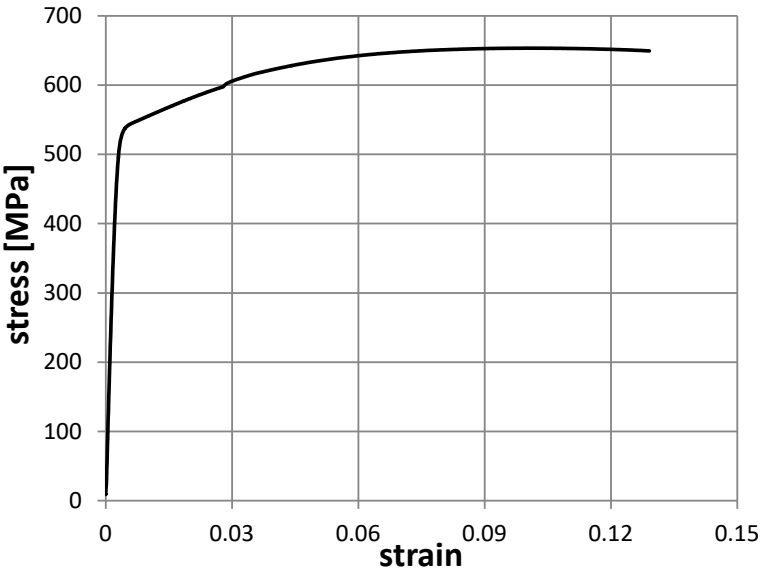

Figure 5: Stress-strain curve for the X70 steel material of the spiral-welded pipe, tested by SZMF [39].

The test configuration is shown in Figure 6a, corresponding to a four-point bending set-up, as already presented schematically in Figure 4, where the distance L between the two loads is equal to 4 meters.

Numerical simulations are conducted for the above spiral-welded pipe subjected to pressurized bending with the corresponding set-up, including a first loading step of hydrotesting (pressure increase up to the yield pressure level), followed by an unloading step. In the absence of initial wrinkling measurements, the imperfection amplitude w_0 is chosen equal to 1%, as a representative value according to the data reported in [36], and it will also be employed in the parametric study to be presented in the next section. Residual stresses have been computed from the numerical simulation of cold bending process, outlined in the Appendix, considering the parameters of the spiral geometry, and assuming an initial coil diameter equal to 1000 mm, which is a typical value for coils.

In Figure 6b, the shape of the deformed pipe is shown, with two bulging buckles near the location where the loads are applied. The numerical simulations confirm pipe failure in the form of two local bulging buckles at the vicinity of the loads. The buckles have a shape reminiscent of the "elephant's foot" buckle that often occurs at the bottom of cylindrical liquid storage tanks under meridian compression. A comparison of the buckled shape obtained numerically with the one obtained experimentally is offered in Figure 7b, whereas Figure 8 plots the average force and the average displacement from the two locations where the forces are applied. The results show a very good comparison between experiments and numerical results.

(a)

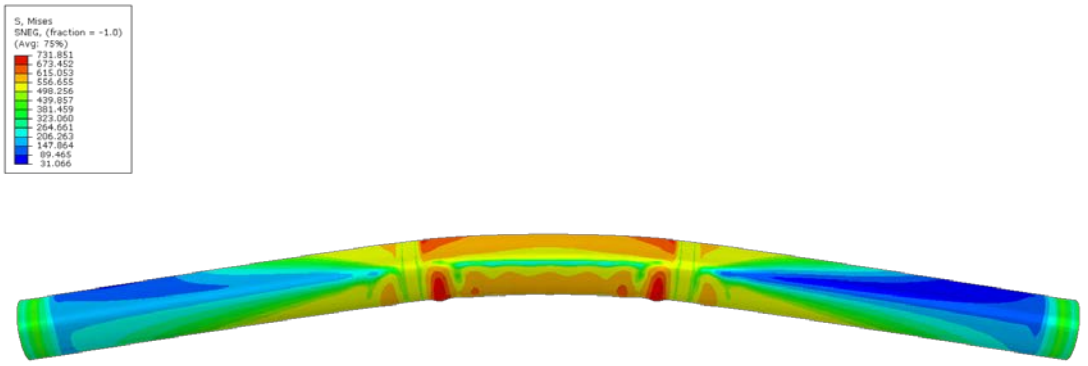

(b)

Figure 6: Comparison of buckled shape from (a) the experiment performed by SZMF [39] and (b) the present numerical simulation.

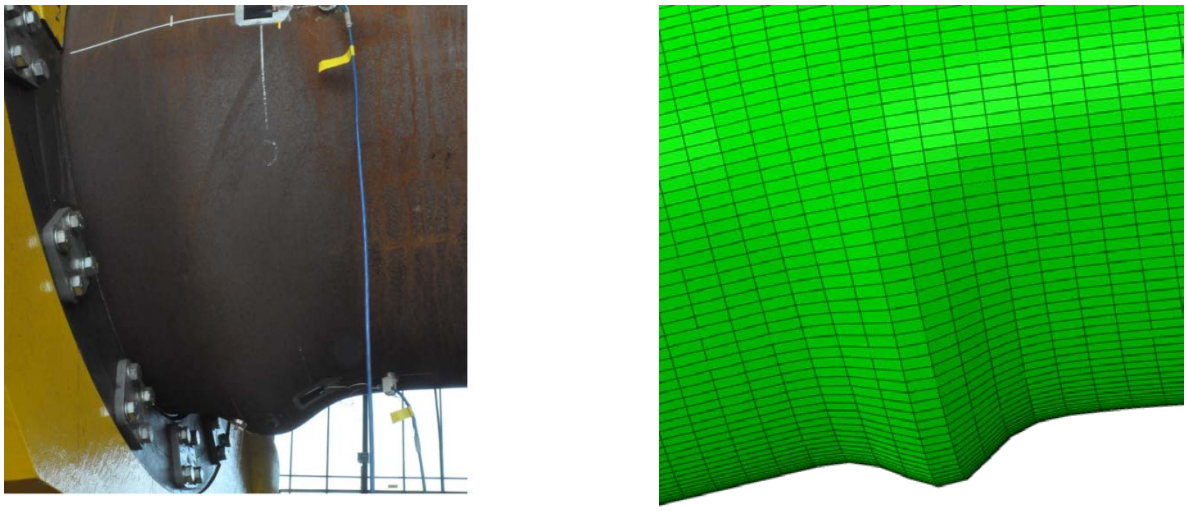

Figure 7: Buckled pipe shape at the vicinity of load application; present numerical simulation (right), compared with the shape from experiment (left) [39].

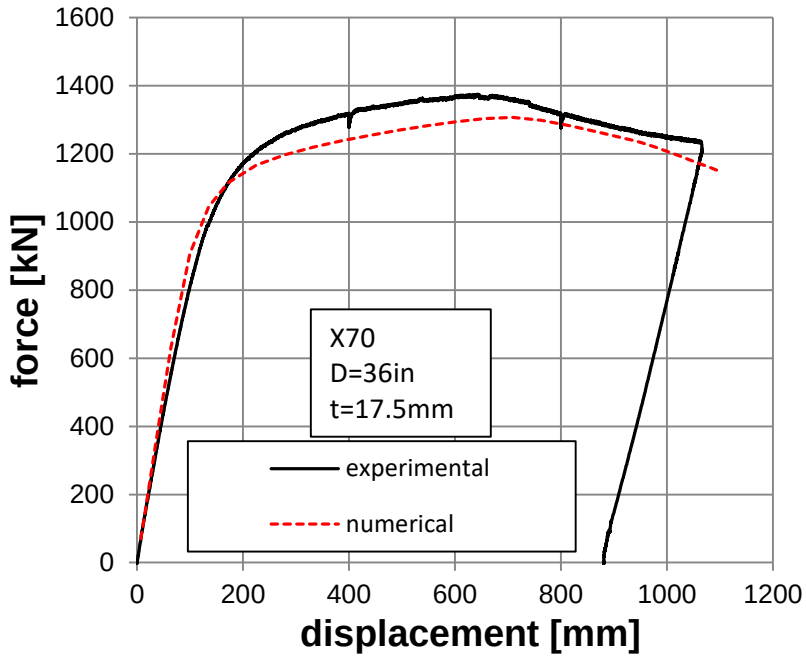

Figure 8: Comparison of force-displacement curve between present numerical simulation and the experimental results [39].

NUMERICAL RESULTS

Two spiral-welded pipes are considered in the numerical parametric study. The first pipe, referred to as Pipe I, has the characteristics of the 36-inch-diameter pipe tested in the SZMF experiment **Σφάλμα! Το αρχείο προέλευσης της αναφοράς δεν βρέθηκε.**, and the pipe thickness is equal to 17.1 mm ($D/t =$ 53). The second pipe, referred to as Pipe II, is a 48-inch-diameter pipe with 17.5 mm thickness, manufactured with a spiral angle of 27.35 degrees, and a coil width equal to 1760 mm. It is assumed that the pipes are made of X70 steel material, which follows the stress-strain curve of Figure 5. Both pipes are candidates for onshore gas pipeline applications.

The pipes have initial wrinkling (before hydrotesting), equal to 1% of the pipe thickness, and residual stresses calculated from the simulation of the manufacturing process described in the Appendix. The bending loading scheme adopted in the present analysis follows the set-up of Figure 4, with a value of central length L equal to 10 m for pipe I and 13.3 m for pipe II, so that the central part is at least 10 times the pipe diameter.

The numerical results focus on the effects of (a) internal pressure, (b) hydrotesting after manufacturing and (c) "high-low" misalignment at the girth weld on structural response. The results are reported in the form of moment-curvature diagrams, curvature κ of the bent specimen is defined equal to $8\delta/L^2$, where the length L and the mid-span displacement δ. Emphasis is given on the value of the critical bending curvature κ_C, defined as the curvature at which maximum moment M_{max} occurs. The value of buckling wave length and its dependence on the internal pressure level is discussed, and comparison of the critical bending curvature with empirical equations, employed in pipeline design, is also conducted. Furthermore, results are presented in terms of the development of local strains at critical locations.

Effect of internal pressure and hydrotesting

The influence of the level of internal pressure on the structural response of spiral-welded pipes, is examined first, and the results are depicted in Figure 9 and in Figure 10 in terms of the moment-curvature diagrams, including the effects of hydrotesting. Furthermore, the values of maximum bending moment and the corresponding "critical" (buckling) curvature are plotted in Figure 11 and Figure 12.

The main observation from those numerical results is that the critical curvature κ_C increases significantly with increasing level of internal pressure. This increase is similar, yet somewhat less pronounced, to the one observed in the experimental results of ref. [28]. It is noted that the small-scale

specimens in [28] are seamless stainless steel pipes, which implies a higher hardening modulus and very small (negligible) residual stresses.

An extensive investigation on the influence of hydrotest on the structural response of spiral-welded pipes is presented in [42]. The results have shown that hydrotest reduces the residual stresses from the manufacturing process and, as a result, it affects pressurized bending response of the pipe. For relatively low values of internal pressure, hydrotesting reduces the value of the critical curvature κ_C, whereas the effect of hydrotesting at high levels of pressure is not significant. Furthermore, hydrotesting increases bending moment capacity due to the strain hardening induced in the pipe.

The numerical results are compared with two empirical equations, adopted by current design standards. The first equation has been proposed by Gresnigt [19], and expresses the critical (compressive) bending strain in terms of pipe geometry and the level of pressure:

$$\varepsilon_C = 0.5\frac{t}{D} - 0.0025 + 3000\left(\frac{pD}{2tE}\right)^2 \quad (1)$$

Gresnigt's equation is based mainly on the numerous tests performed in the '80s, as described in [19], and it has been adopted by Canadian standard CSA Z662 [40]. The second equation for the bending capacity of internally-pressurized pipes is given by the following empirical design equation, proposed by DNV standard DNV-OS-F101 [41]

$$\varepsilon_C = 0.78\left(\frac{t}{D} - 0.01\right)\cdot\left(1 + 5.57\frac{p}{p_b}\right)\alpha_h^{-1.5}\alpha_{gw} \quad (2)$$

where α_h is the strain hardening factor and α_{gw} is the girth weld factor, herein taken equal to 0.70 and 0.93 respectively. In both equations, p is the internal pressure and p_b is the burst pressure of the pipe calculated by equation (3):

$$p_b = \frac{2t}{D-t} f_{cb}\frac{2}{\sqrt{3}} \quad (3)$$

where f_{cb} is the minimum of σ_Y (yield stress) and $\sigma_u/1.15$ (σ_u is the tensile strength of the material). Upon calculation of the critical bending strain ε_C, the critical curvature κ_C can be computed from equation (4):

$$\kappa_C = 2\varepsilon_C/D \quad (4)$$

In addition to the expression for the critical bending curvature κ_C, a prediction for the ultimate bending moment $M_{\max}$ is offered by DNV standard [41] in terms of the level of pressure by an interaction formula, which is written below in a format compatible with our notation and setting safety factors equal to 1:

$$M_{\max} \le M_P \sqrt{\alpha_c{}^2 - \left(\alpha_p \frac{p}{P_b} \right)^2} \tag{5}$$

where $a_c = (1-\beta) + \beta \frac{\sigma_u}{\sigma_Y}$, $a_p = 1-\beta$, and $\beta = \frac{60 - (D/t)}{90}$

Figure 11a and Figure 12a show that the empirical equations in [19] [40] [41] offer reliable, yet somewhat conservative, estimates of the critical bending curvature κ_C. Furthermore, the maximum moment $M_{\max}$ predictions from DNV standard [41] in Figure 11b and Figure 12b are rather conservative, mainly because of strain-hardening, which is not accounted for in this empirical equation.

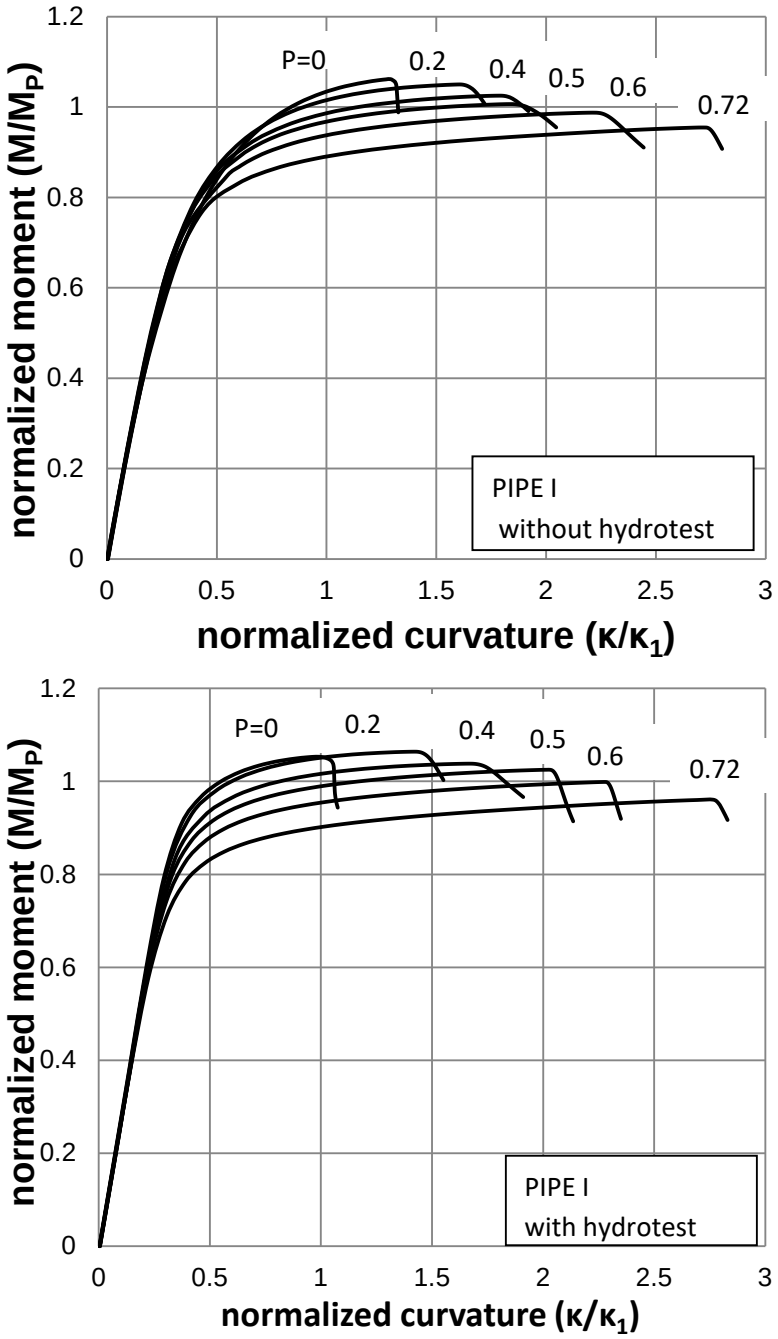

Figure 9: Pressurized bending response of pipe I; (a) without hydrotesting, (b) with hydrotesting.

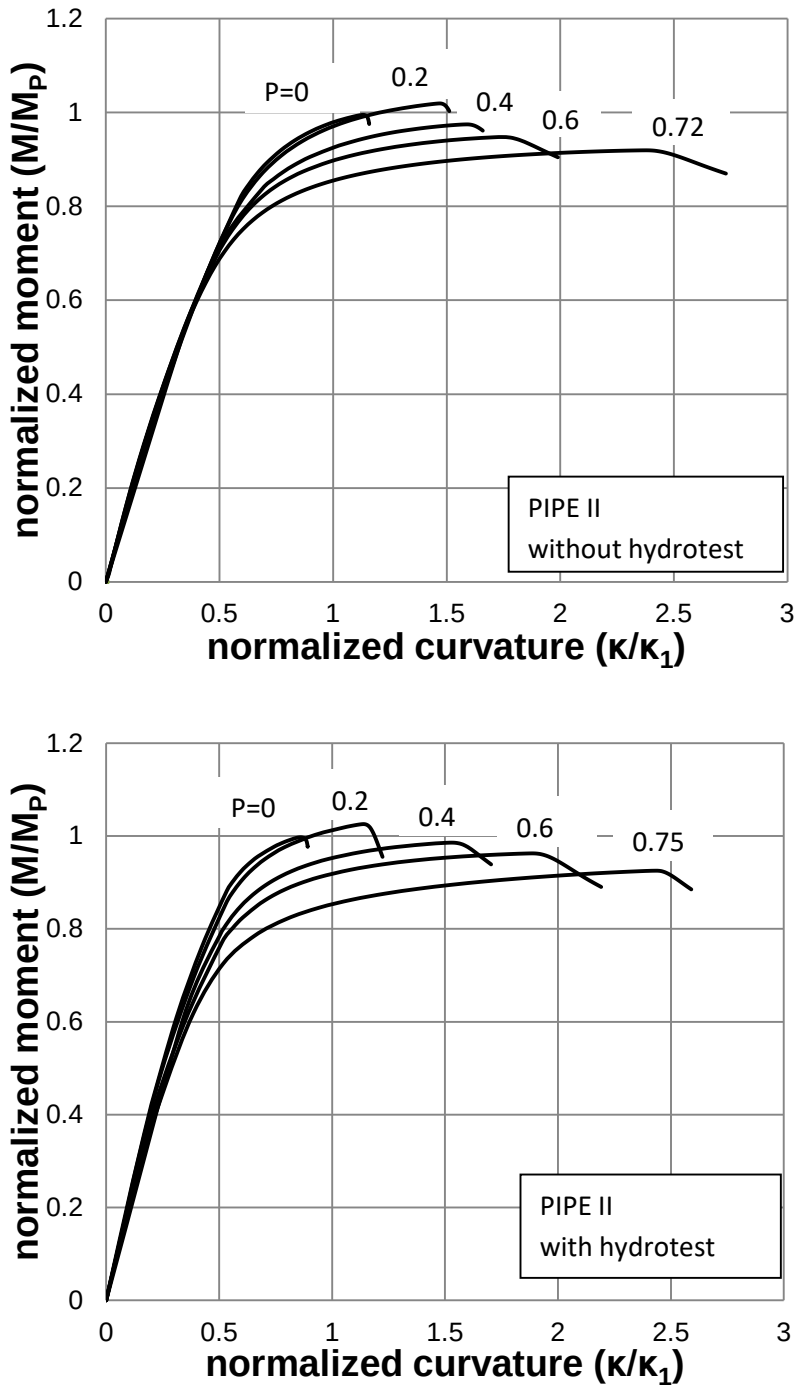

Figure 10*:* Pressurized bending response of pipe II; (a) without hydrotesting, (b) with hydrotesting.

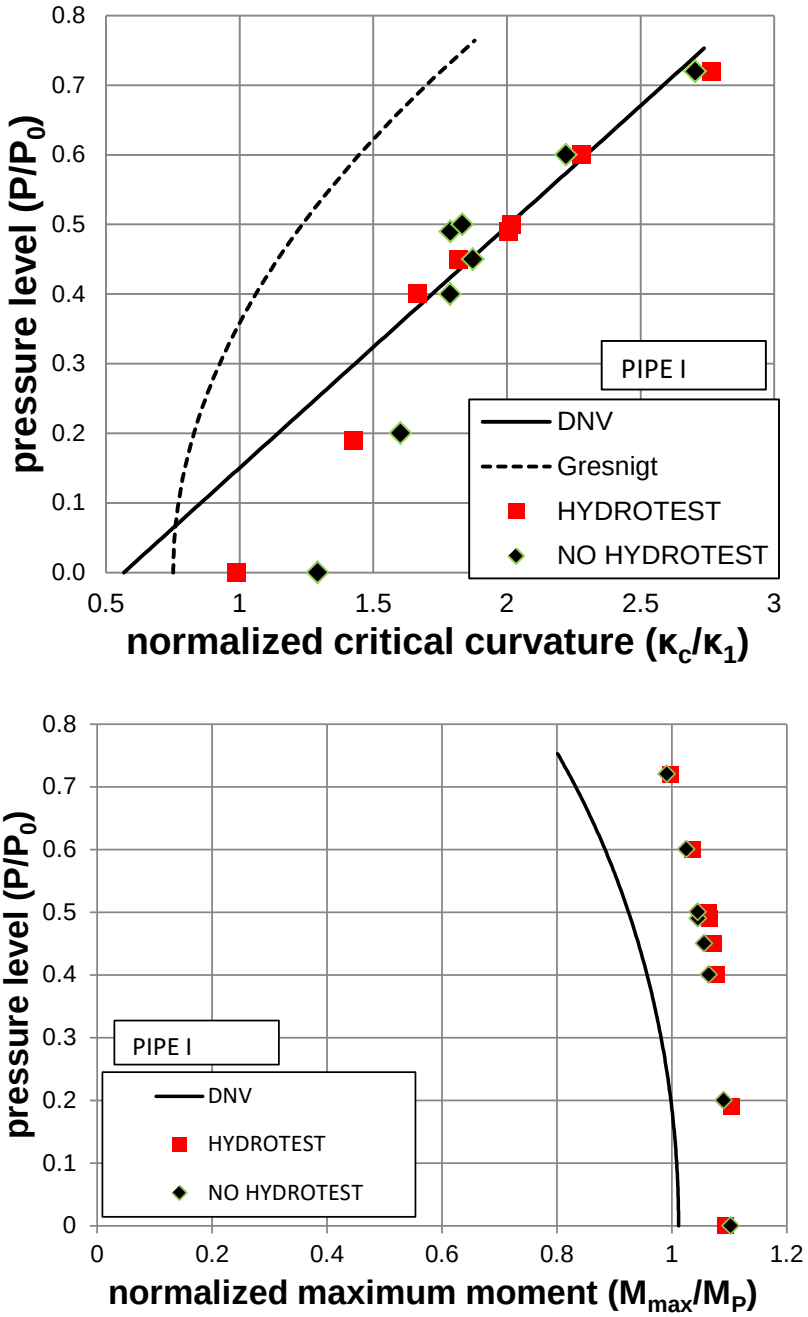

Figure 11: Variation of bending capacity in terms of internal pressure level for Pipe I and comparison with empirical equations; (a) critical bending curvature and (b) maximum bending moment.

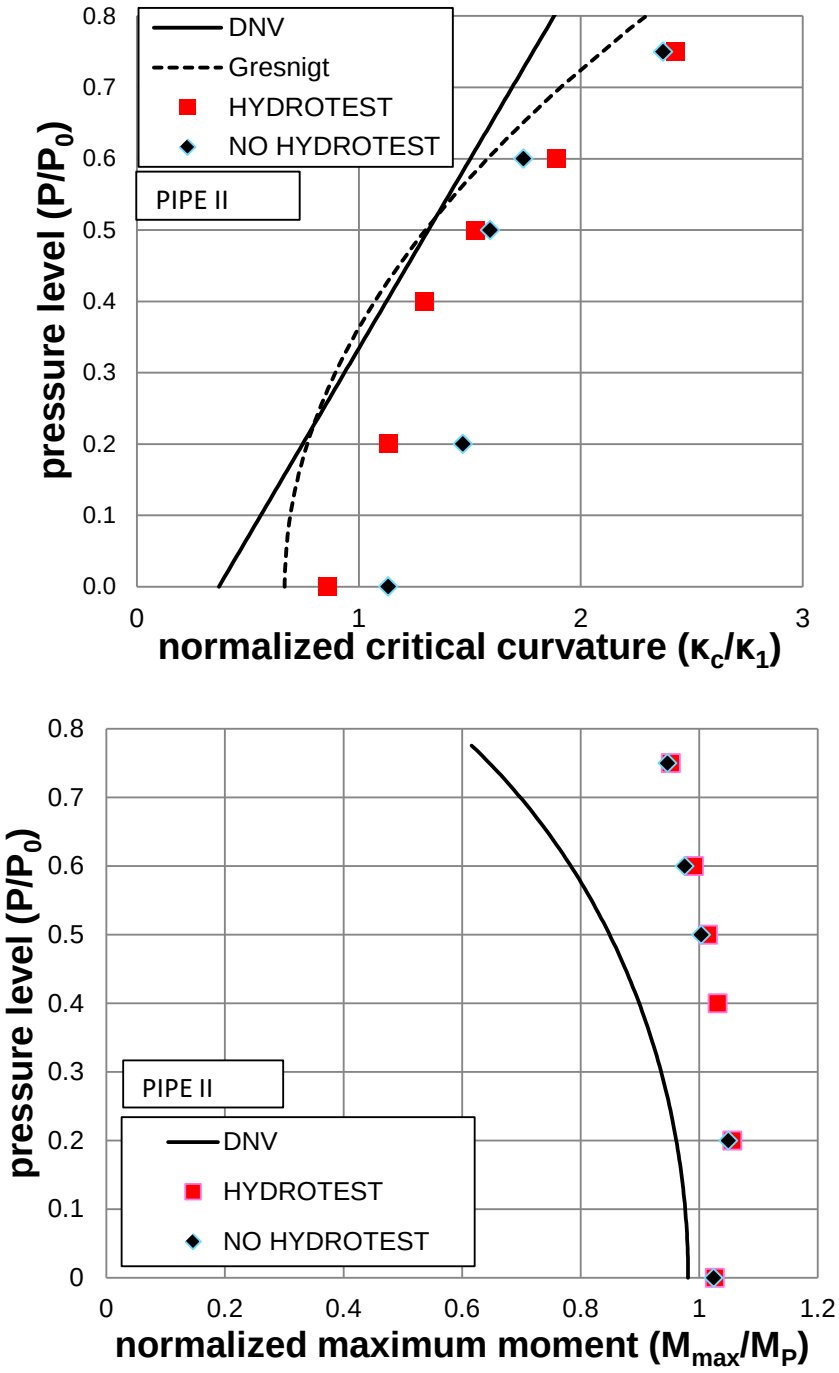

Figure 12: Variation of bending capacity in terms of internal pressure level for Pipe II and comparison with empirical equations; (a) critical bending curvature and (b) maximum bending moment.

Buckling wavelength and imperfection sensitivity

The value of half-wave length L_{hw} of the buckled pattern, normalized by $\sqrt{Dt}$, obtained from the numerical results and measured as ***Figure 3*** shown, is plotted in Figure 13, in terms of different levels of internal pressure. A small decrease of the L_{hw} value is observed with increasing values of internal pressure. Furthermore, the numerical values are compared with the predictions of equation (6), obtained through an analytical solution procedure, described in detail in [8], for the case of elastic elongated cylinders under pressurized bending:

$$\frac{L_{hw}}{L_0} = \sqrt{\frac{1+f}{1+f-3\hat{\kappa}_{cr}^2}} \tag{6}$$

where

$$L_0 = \sqrt{rt}\left[\pi^4 \big/ 12\left(1-\nu^2\right)\right]^{1/4} \tag{7}$$

is the value of the buckling half-wave length under axisymmetric conditions, r is the radius of the cylinder,

$$\hat{\kappa}_{cr} = \kappa_C \big/ \kappa_N \tag{8}$$

is the normalized critical curvature,

$$\kappa_N = t \Big/ \left(r^2\sqrt{1-\nu^2}\right) \tag{9}$$

is a curvature parameter used for normalization purposes, and

$$f = p / p_e \tag{10}$$

is a dimensionless parameter that expresses the level of internal pressure p, with respect to the buckling pressure p_e of an elastic ring subjected to uniform external pressure:

$$p_e = Et^3 \big/ 4r^3(1-\nu^2) \tag{11}$$

The comparison shows a very good agreement between the numerical results and the analytical solution. The results indicate a small variation of the L_{hw} value with increasing pressure levels; the value of L_{hw} can be assumed to remain nearly constant and equal to about $1.2\sqrt{Dt}$.

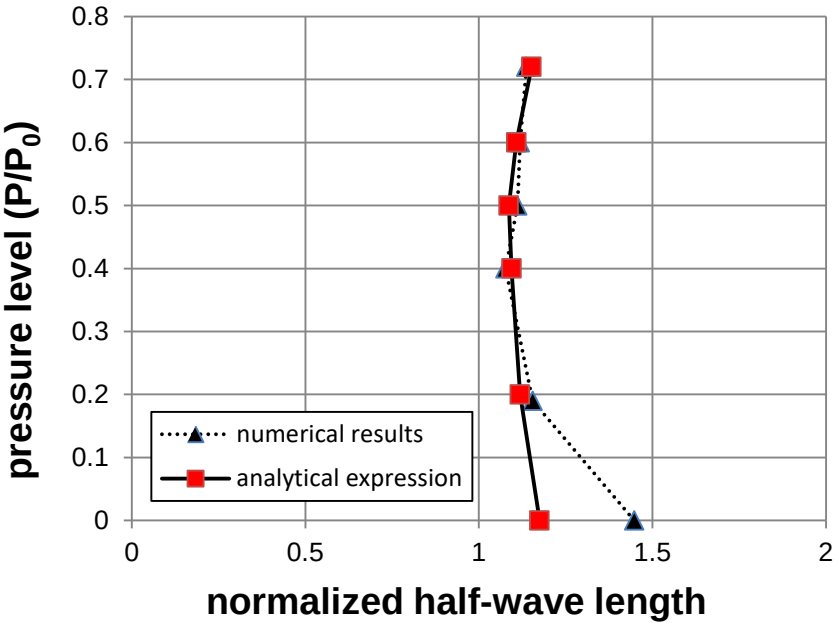

Figure 13: Variation of buckling wave length in terms of the level of internal pressure; comparison with elastic analytical expression.

Buckled shapes

The deformed shapes of pipe I for four different levels of internal pressure are depicted in Figure 14 and Figure 15. For zero pressure, local buckling occurs in the form of an inward "kink" shown in Figure 14a, which is similar to the buckle shown in Figure 1a, and the one reported in the non-pressurized tests reported in [28]. Increasing the level of pressure, the shape of the buckle becomes an outward bulging pattern, as shown in Figure 1b. Furthermore, the deformed shapes of the bent pipe shown in Figure 15 for high-pressure levels (50% and 72% of the yield pressure), indicate that highly-pressurized pipe can be bent at remarkably large curvatures before reaching a local buckling limit state.

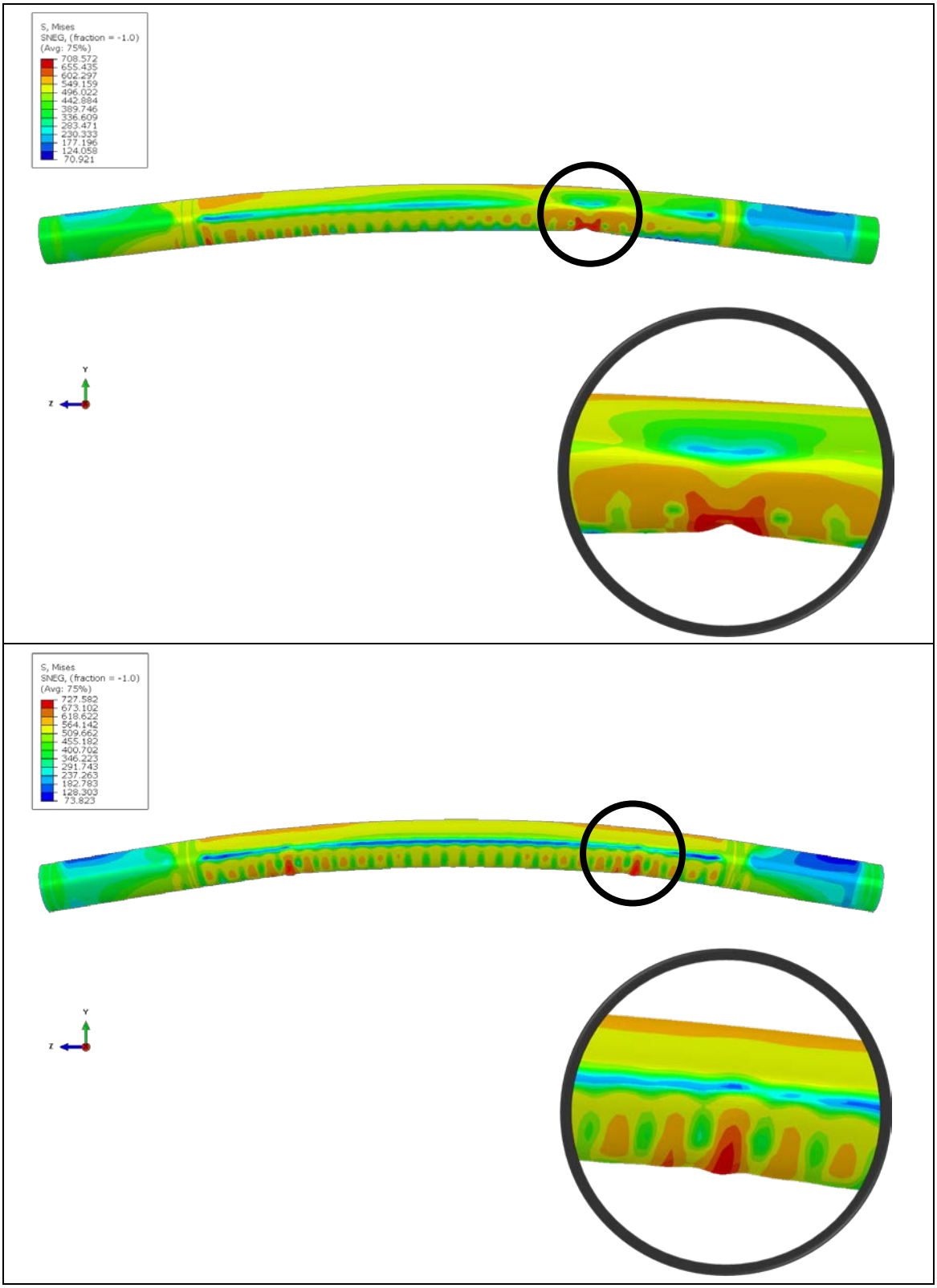

Figure 14: Post-buckling configuration of pipe I, subjected to bending under (a) zero pressure and (b) internal pressure equal to 19% of yield pressure.

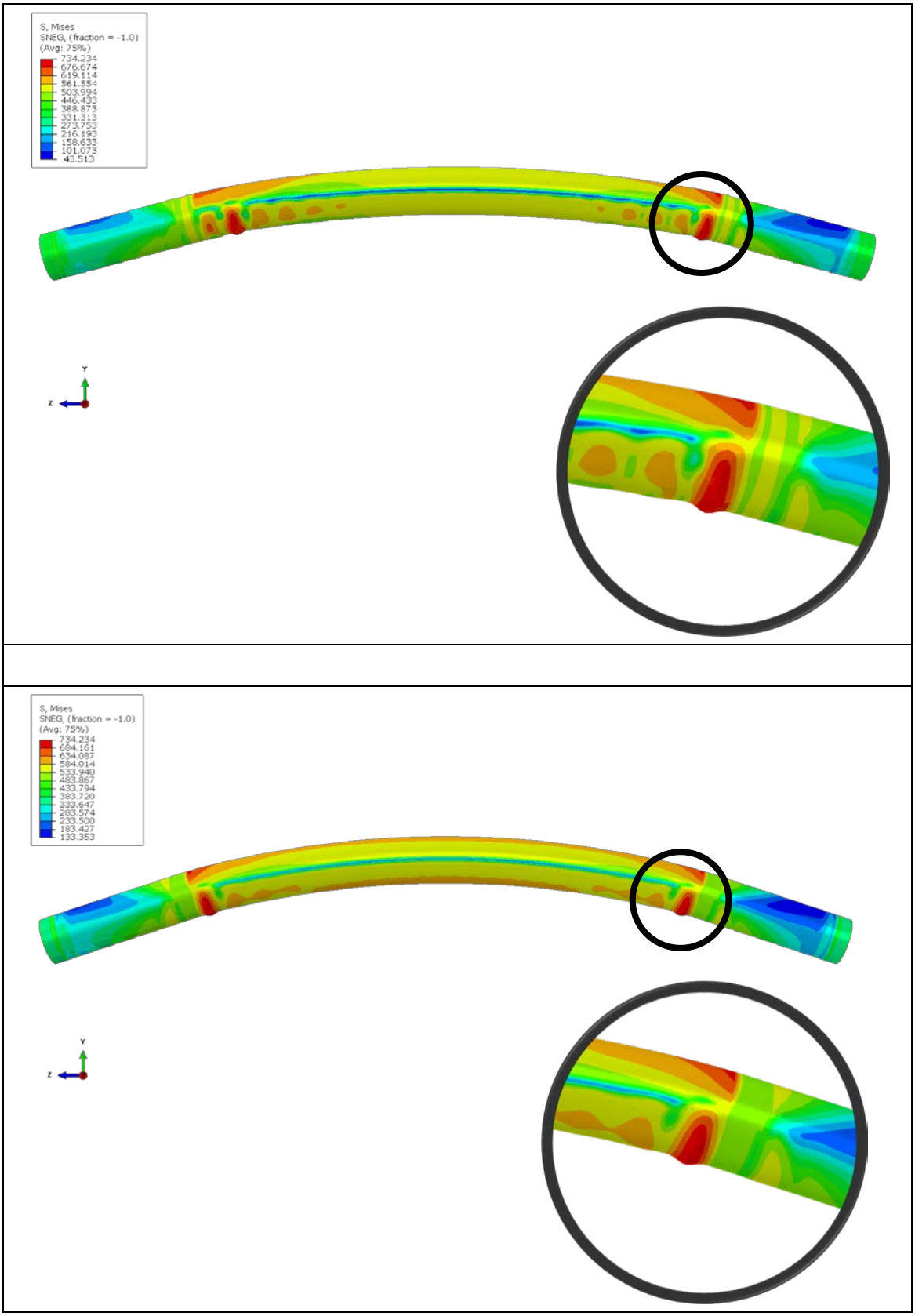

Figure 15: Post-buckling configuration of pipe I, subjected to bending under high levels of internal pressure, equal to (a) 50% of yield pressure and (b) 72% of yield pressure.

Imperfection sensitivity

The influence of geometric initial imperfections, in the form of short wave wrinkles, on the pipe response under pressurized bending conditions is also examined. In the present analysis, wrinkles are considered in the initial configuration of the model as described in a previous section of the paper. The normalized moment-curvature diagrams of pipe II for different level of pressure are shown in Figure 16 and Figure 17 respectively and for different values of imperfection amplitudes. It is observed that for the lower value of pressure ($p/p_0 = 20\%$) the effect of imperfection is slightly more pronounced. Nevertheless, it should be noted that for this range of imperfection amplitude, the influence of initial wrinkling on the pressurized bending behavior of pipes is relatively small.

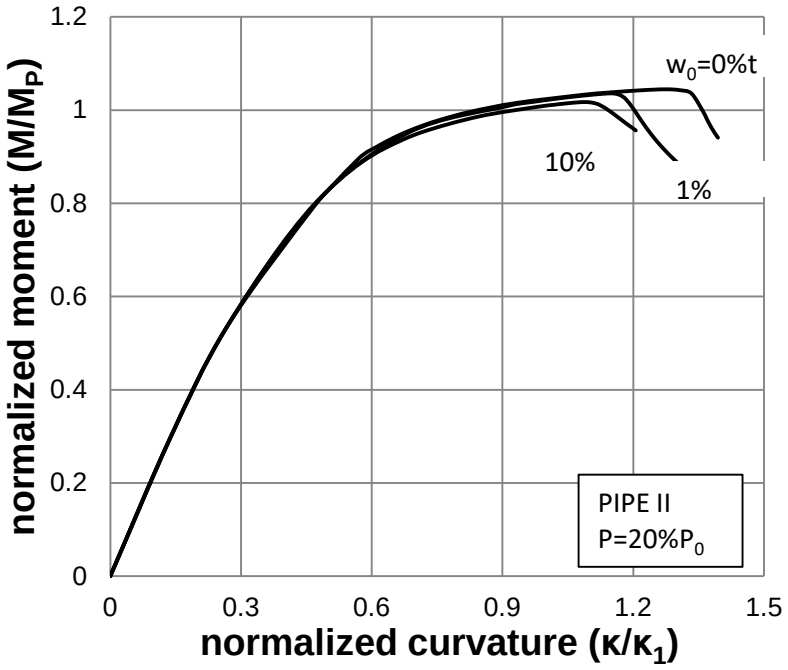

Figure 16: Pressurized bending response of pipe II for different imperfection amplitudes ($p/p_0 = 20\%$).

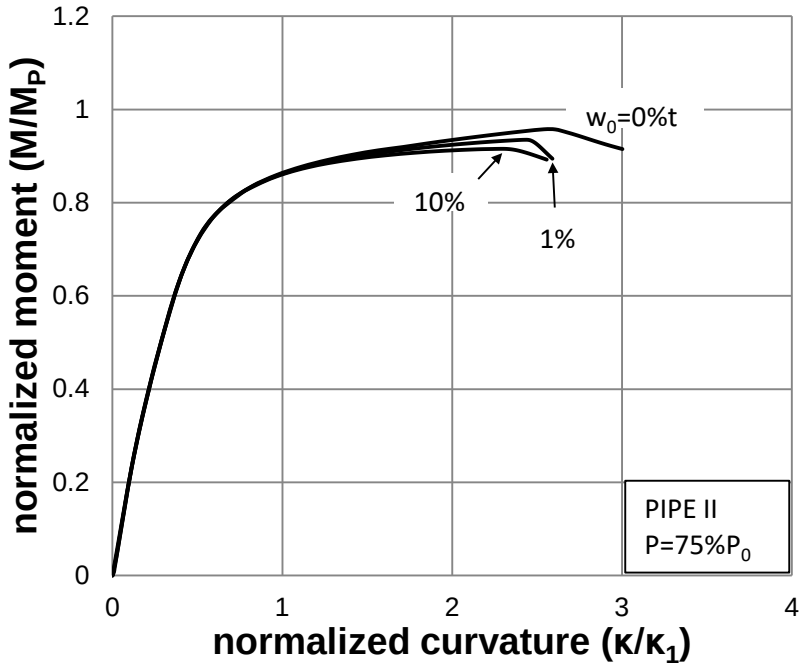

Figure 17: Pressurized bending response of pipe II for different imperfection amplitudes ($p/p_0 = 75\%$).

Influence of "high-low" girth weld misalignment

The influence of girth weld misalignment on the pipe bending response under pressurized bending conditions is also examined. This is a typical geometric imperfection in the field welds of steel pipelines, often referred to as "high-low" or "hi-lo" imperfection. The finite element model used in this case is based on the simulation procedure described in section "Numerical Model Description". To simulate this "hi-lo" weld misalignment, in the initial configuration of the finite element model, all nodes on one side of the weld location is translated in the y direction by a small offset e , as shown in Figure 18. The value of this offset e is considered up to 40% of pipe wall thickness. To maximize the effects of "high-low" imperfection, bending is applied on the y-z plane (Figure 18), which contains the maximum misalignment around the circumference. Figure 19 and Figure 20 show the effect of girth-weld misalignment e/t on the bending response of pressurized pipe I and pipe II respectively, for a high level of internal pressure. The numerical results indicate a substantial reduction in the value of bending deformation capacity, expressed in terms of the critical curvature κ_C. According to DNV-OS-F101 standard [41], the maximum allowable value of misalignment is equal to 10% of pipe wall thickness, and therefore, the corresponding point on the moment-curvature diagram is of particular importance. In Figure 19 and Figure 20, the buckling point associated with this allowable value of misalignment is marked with an arrow (↓), and the corresponding critical curvature κ_C is significantly lower than the one corresponding to zero misalignment. The effect of

girth weld misalignment on pipe bending behavior is more pronounced in the case of lower pressure levels. The main conclusion from the numerical results in those diagrams is that the presence of girth-weld misalignment may reduce significantly the bending deformation capacity of a steel pipe. ~~It is interesting to compare~~ The numerical results are compared with the predictions of the empirical equation of DNV-OS-F101 standard [41]; for the case of pipe I (Figure 19), the normalized critical curvature κ_C corresponding to 10% weld misalignment (maximum allowable in DNV-OS-F101) is equal to 2.12, while the DNV-OS-F101 standard predicts a value of 2.64, whereas for the case of pipe II (Figure 20), the normalized critical curvature κ_C equal to 1.86, while the DNV-OS-F101 standard predicts a value of 1.79.

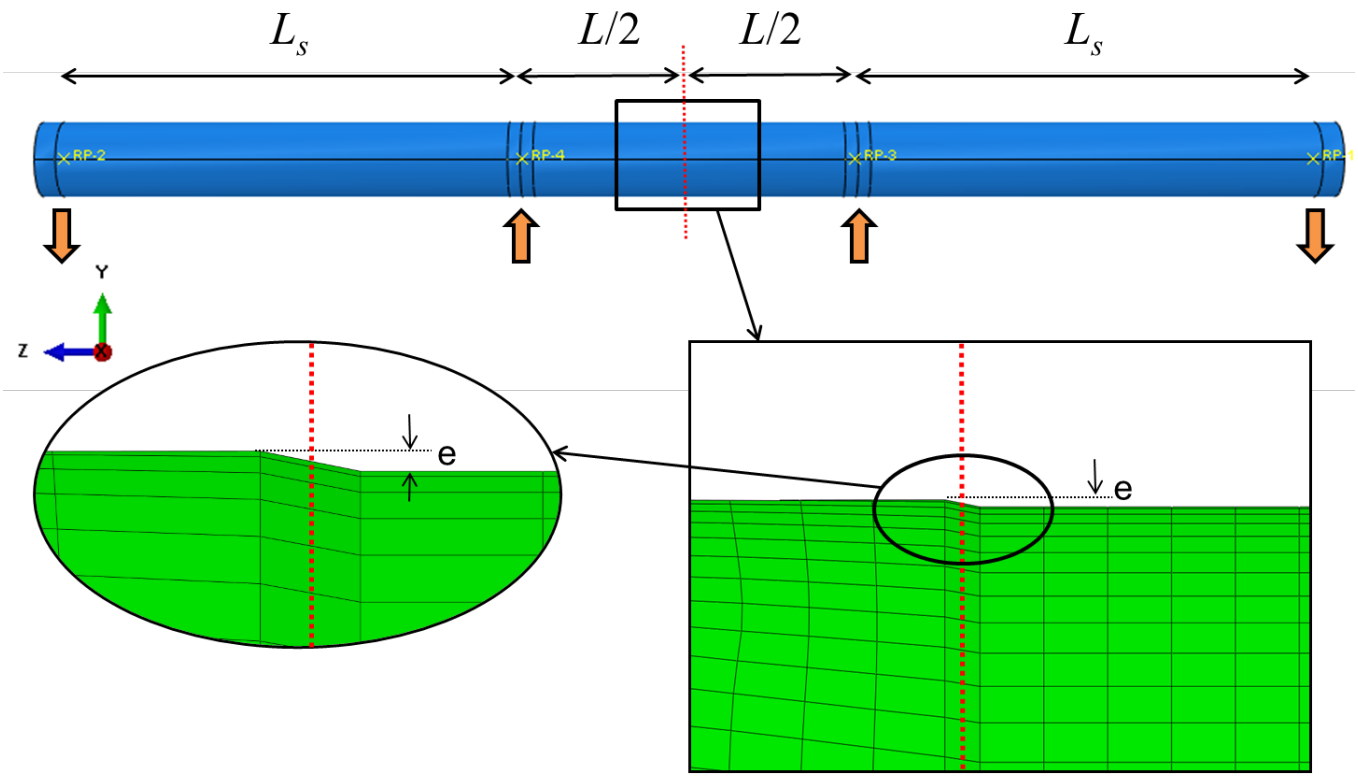

Figure 18: Four-point bending loading pattern for pipe bending and detailed close up of the mesh in the position of misalignment.

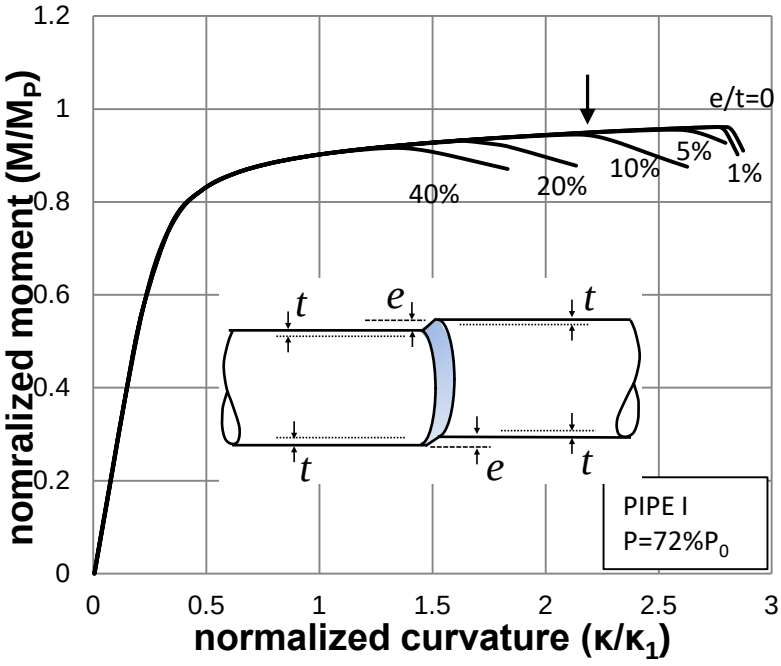

Figure 19: Effect of "high-low" (h/l) girth weld misalignment on bending response of pipe I; pressure at 72% of yield pressure. Arrow (↓) denotes the maximum curvature for $h/l =$ 10% (DNV allowable).

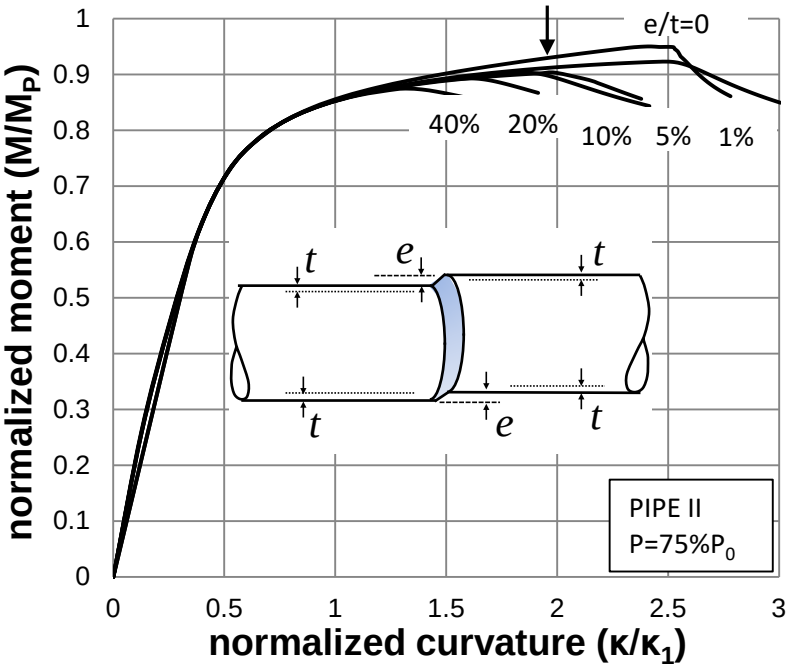

Figure 20: Effect of "high-low" (h/l) girth weld misalignment on bending response of pipe II; pressure at 75% of yield pressure. Arrow (↓) denotes the maximum curvature for $h/l =$ 10% (DNV allowable).

Evolution of local strains

The previous numerical results referred mainly to global bending response, expressing the mechanical behavior of the bent pipes in terms of the corresponding moment-curvature diagrams, as well as the buckling wave length. In addition to this information, the local strains developed at the buckled area are of particular importance for the integrity of pressurized pipes; high local strains may cause fracture of the pipe wall with catastrophic consequences. The local strains are shown in Figure 21, Figure 22, and Figure 23, for zero pressure, 50% of yield pressure and 72% of yield pressure respectively. In Figure 21a,b, Figure 22a,b, and Figure 23a,b, the evolution of strains along the most critical (most compressed) pipe generator is depicted, both on the inner and the outer surface. In particular, four stages of deformation are shown, defined in Figure 21e, Figure 22e, and Figure 23e; stages (1) and (2) correspond to prebucking configurations, stage (3) is the critical (buckling) stage corresponding to the maximum bending moment and stage (4) is into the post-buckling regime. The variation of axial strain along the critical generator is shown in Figure 21c,d, Figure 22c,d, and Figure 23c,d, at the inner and the outer surface, for the three pressure levels under consideration.

A first observation from those graphs is the difference between the strains at the inner and outer pipe surface of the pipe wall. In the three cases examined, the strains at the inner surface are higher than the strains at the outer surface, and this is attributed to pipe wall bending; Furthermore, local strains at the stage of local buckling [stage (3)] are significantly higher than the bending strain predicted by the empirical design equations (1) and (2), discussed in the previous paragraph. More specifically, the numerical results in Figure 21c,d, Figure 22c,d, and Figure 23c,d, indicate that the average values of maximum compressive strain (from outer and inner surface) depicted in those figures are equal to 2.4%, 4.3% and 5.3% for the three levels of pressure under consideration, which are considerably higher than the ones predicted by equations (1) and (2); they are 0.7%, 1.15%, 1.64% from equation (1) for the three levels of pressure under consideration, and equal to 0.53%, 1.86%, 2.47% from equation (2).

The numerical results depicted in those graphs also indicate a wavy variation of strain along the most compressed generator of the bent pipe. This is an indication of a first bifurcation of the pipe configuration into a wrinkling pattern, which occurs at an early stage of bending. However, this first bifurcation appears to be structurally stable, so that bending resistance continues to increase beyond this stage. With further continuation of bending deformation, one of the wrinkles becomes dominant, and the deformation localizes at this wrinkle, resulting in the formation of a local “kink” or “bulge”, associated with pipe structural failure

and loss of structural strength. A similar observation has been reported in [28], and in compressive load tests performed by Parquette *et al*. [18].

Upon local buckling formation, the cross-sectional bending resistance of the pipe at the buckled cross-section is substantially reduced, resulting in the development of high local strains at both sides of the bent pipe (referred to as “intrados” and “extrados” as shown in **Figure 24**). With continuing bending deformation beyond the buckling stage, the local bulging buckle results in a folding pattern at the compression side, which increases significantly the local strains due to local bending of the pipe wall. The evolution of strains at point A, which is the crest of the bulging configuration of pipe I, is shown in Figure 24, in terms of the applied bending curvature. The results refer to internal pressure level equal to 72% of yield pressure and indicate that, upon local buckling formation, the hoop strains at both surfaces of the pipe wall increase very rapidly due to the outward displacement associated with bulging. Furthermore, the axial strain at the inner surface of pipe wall also increases very rapidly, whereas the axial strain at the outer surface starts decreasing, due to the development of significant pipe wall bending strains in the bulging area.

Due to the reduction of cross-sectional resistance, apart from the development of high strains at the compression side of the bent pipe (intrados), significant levels of strain also develop at the tension side (extrados) of the bent pipe. The axial and hoop strains at point B of pipe I are depicted in Figure 25, at both the inner and outer surface. Point B is located at the tension side of the buckled cross-section (pipe extrados), opposite of point A. In that location, there is very little difference between the strain values at the inner and the outer pipe wall surface, due to the lack of any local bending. The most important observation is the significant increase of axial strains upon the occurrence of local buckling. This increase implies the rapid development of very high axial strain at this location, resulting in possible fracture of the pipe wall and loss of containment, which has been observed experimentally [20] [32].

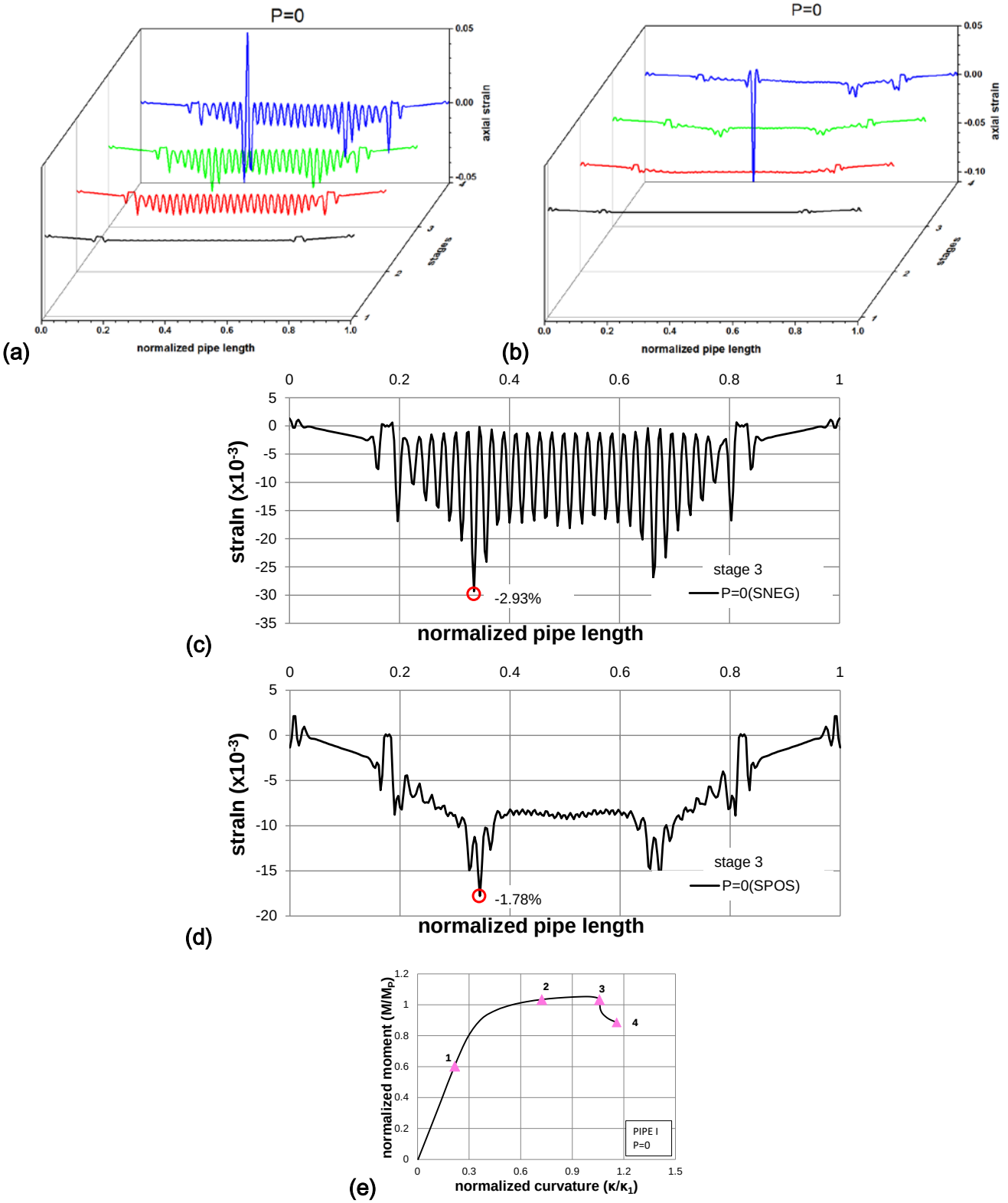

Figure 21: Evolution of strains along the most compressed generator of pipe I (zero pressure conditions); (a) and (b) refer to stages 1, 2, 3 and 4 shown in the diagram of (e) for inner and outer pipe wall surface respectively; (c) and (d) show in detail strain variation along the pipe at the onset of buckling (stage 3).

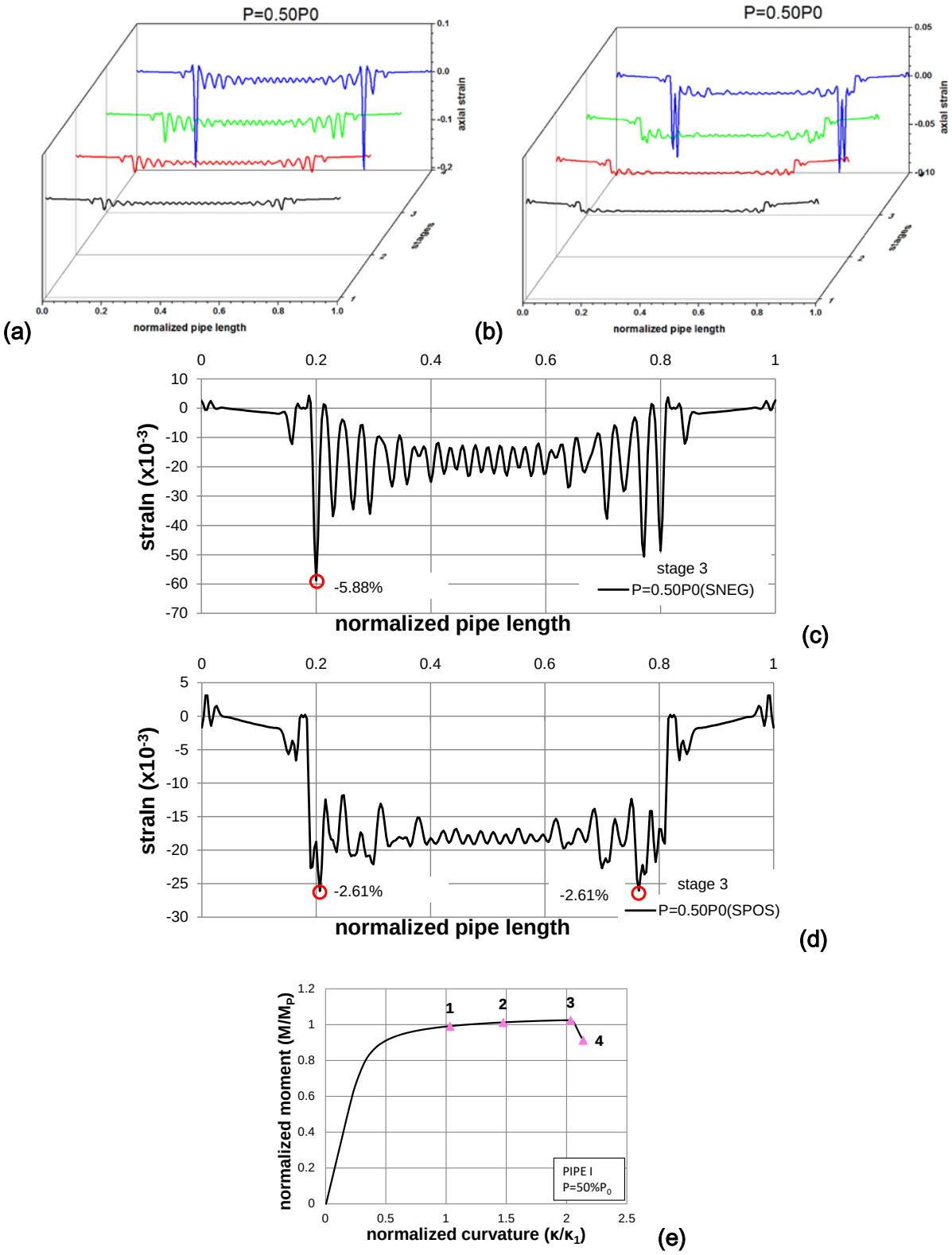

Figure 22: Evolution of strains along the most compressed generator of pipe I (pressure equal to 50% of yield pressure); (a) and (b) refer to stages 1, 2, 3 and 4 shown in the diagram of (e) for inner and outer pipe wall surface respectively; (c) and (d) show in detail strain variation along the pipe at the onset of buckling (stage 3).

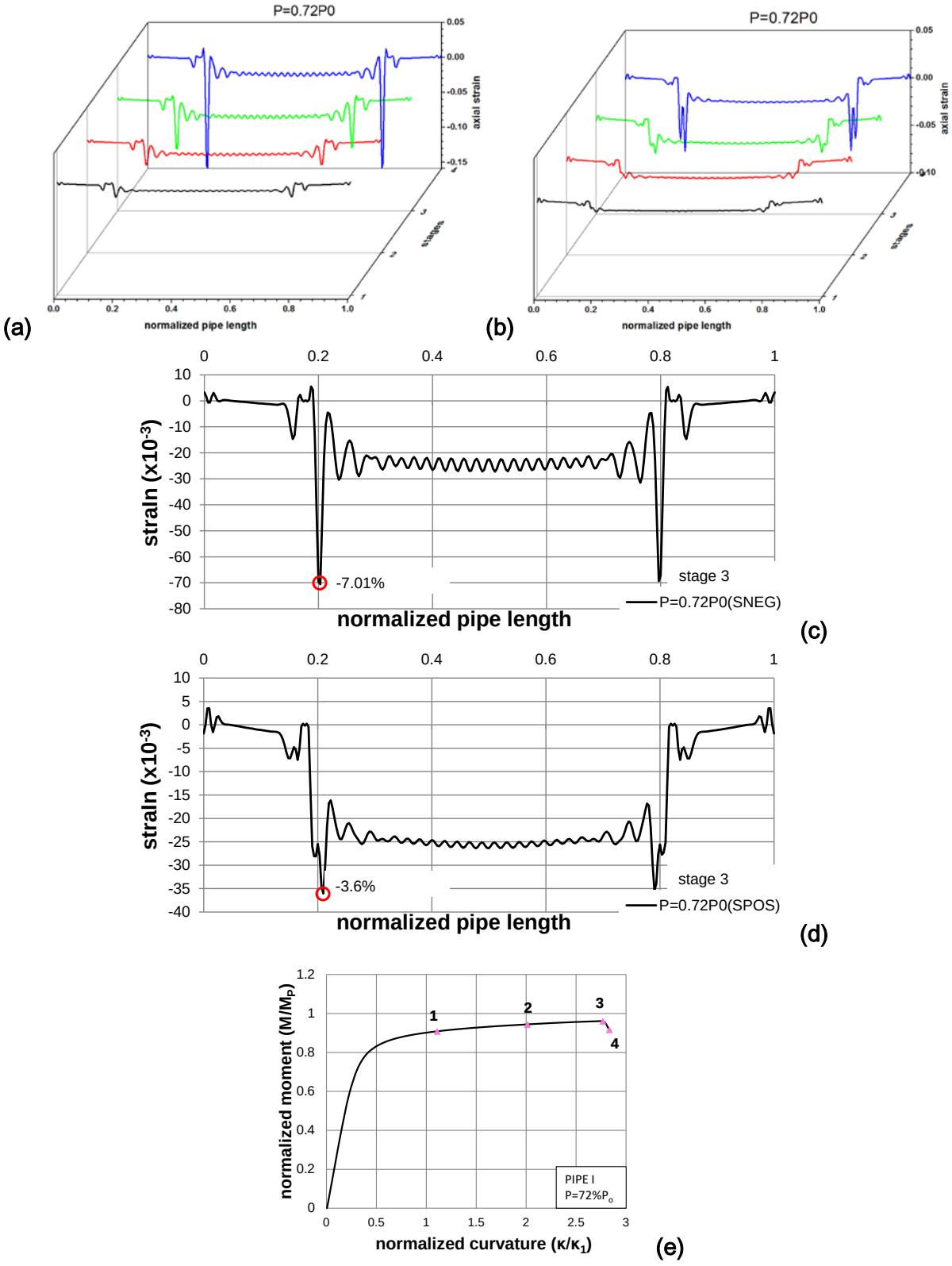

Figure 23: Evolution of strains along the most compressed generator of pipe I (pressure equal to 72% of yield pressure); (a) and (b) refer to stages 1, 2, 3 and 4 shown in the diagram of (e) for inner and outer pipe wall surface respectively; (c) and (d) show in detail strain variation along the pipe at the onset of buckling (stage 3).

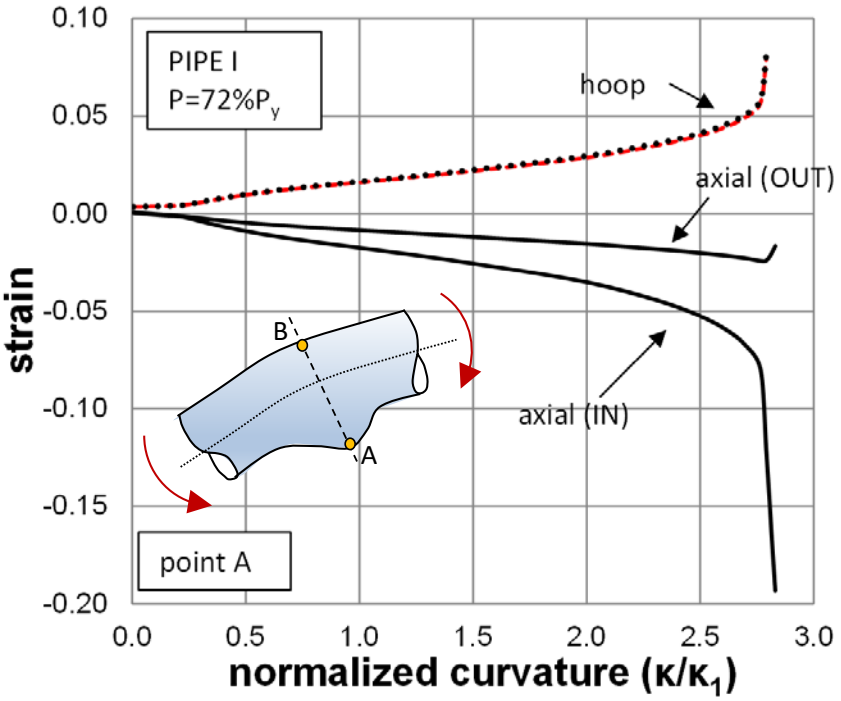

Figure 24: Evolution of strains at point A of the buckled cross-section (intrados) of bent pipe I in the axial and the hoop direction (inside and outside surface of the pipe); bending under pressure equal to 72% of yield pressure.

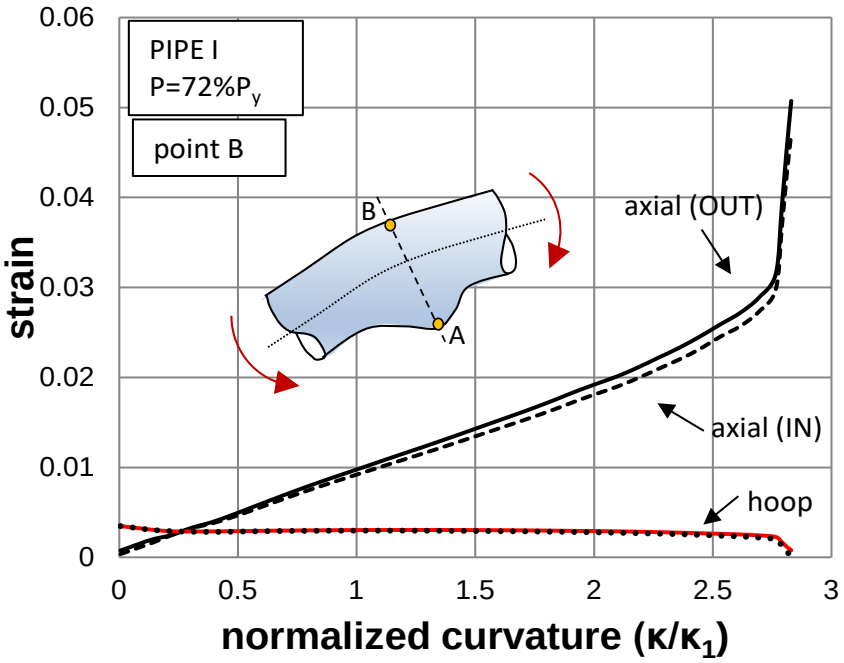

Figure 25: Evolution of strains at point B of the buckled cross-section (extrados) of bent pipe I in the axial and the hoop direction (inside and outside surface of the pipe); bending under pressure equal to 72% of yield pressure.

CONCLUSIONS

A numerical investigation has been performed, on the structural behavior of large-diameter spiral-welded steel pipes, subjected to pressurized bending. Two pipes have been analyzed; a 36-inch-diameter pipe with diameter-to-thickness ratio D/t equal to 53, and a 48-inch-diameter pipe with D/t equal to 69.3, both candidates for onshore pipeline applications. The numerical simulation is based on advanced finite element tools, which account for the spiral cold-bending manufacturing process, and have been verified against available experimental results.

The numerical results indicated that bending deformation capacity increases in the presence of internal pressure. For pressure levels exceeding 70% of yield pressure, the critical bending curvature κ_C has been calculated more than two times greater than the corresponding curvature at zero pressure conditions. Furthermore, the buckling shape in the presence of pressure has a bulging pattern, instead of a local inward kink observed in zero or low pressure conditions. Moreover, hydrotesting has a non-beneficial effect on the bending response, reducing the value of the critical bending curvature κ_C.

Comparison of numerical results with empirical equations, widely used in pipeline design, showed that those equations can provide safe estimates of critical curvature and ultimate bending moment. Furthermore, the value of buckling wavelength was found to compare well with the predictions from an analytical methodology for elastic elongated cylinders, presented elsewhere. The sensitivity of the critical curvature value on initial wrinkling amplitude has been found relatively small for highly-pressurized pipes and for wrinkling amplitude up to 10% of pipe wall thickness, whereas weld misalignment may impose a severe reduction on bending deformation.

Special attention has been given on the development of local strains at the buckled cross-section. It was found that due to local folding of the buckling pattern, significant local strains develop. At the onset of buckling, those local strains are significantly higher than the ones predicted by simple beam bending theory using the pipe bending curvature. In addition, high tensile strains also develop at the tension side of the buckled section. In the case of pressurized bending, those tensile strains may cause fracture of the pipe wall.

The results from the present study appear to support the argument that, in terms of their bending capacity against buckling, large-diameter spiral-welded steel pipes can be used in demanding onshore pipeline applications, such as geohazard areas.

ACKNOWLEDGEMENTS

The present work has been conducted in the course of SBD-SPIPE project, sponsored by the European Commission through the Research Fund for Coal & Steel (RFCS), Grant Agreement No. RFSR-CT-2013-00025. The authors would like to thank all SBD-SPIPE partners for their fruitful discussions throughout the course of the project. Special thanks go to Salzgitter Mannesmann Forschung GmbH and, in particular, to Dr. Oliver Hilgert, for providing the test results from the full-scale experiment.

APPENDIX. SIMULATION OF SPIRAL PIPE COLD-BENDING PROCESS

A special-purpose methodology has been developed in ABAQUS/Standard to simulate the cold-bending manufacturing process, with the purpose of calculating the corresponding residual stresses. Those residual stresses are inserted manually as initial stresses in the structural model for pressurized bending computations. The manufacturing process consists of two main steps: (a) de-coiling and (b) spiral cold bending. The de-coiling stage starts with a steel strip of appropriate width, initially at the curved (coiled) configuration shown in Figure 26a. The strip is straightened to a plate as shown in Figure 26a, simulating de-coiling process. Subsequently, the plate is passed through a three-roller system Figure 26b at an appropriate angle that bends the steel plate and forms the spiral configuration. Contact between the coil/strip and the rigid parts is assumed frictionless.

The basic geometric characteristics of the numerical model are depicted in Figure 26. Given the tube diameter D, it is possible to calculate the corresponding forming (spiral) angle a and the coil B width using simple geometric calculations, also shown in Figure 26. Throughout the forming process (decoiling, spiral forming), all material state parameters (stresses, strains) are recorded, and the material state variables after manufacturing, are inserted manually as initial conditions in the finite element structural model for pressurized bending calculations (described in the present paper). It is also noted that the manufacturing process is associated with reverse plastic deformations, and therefore, an in-house cyclic-plasticity constitutive model has been employed that accounts for both the plastic plateau and the Bauschinger effect of the steel material. For a more detailed presentation of the finite element simulation of spiral forming, as well as on the in-house plasticity model, the reader is referred to the paper by Chatzopoulou *et al.* [42].

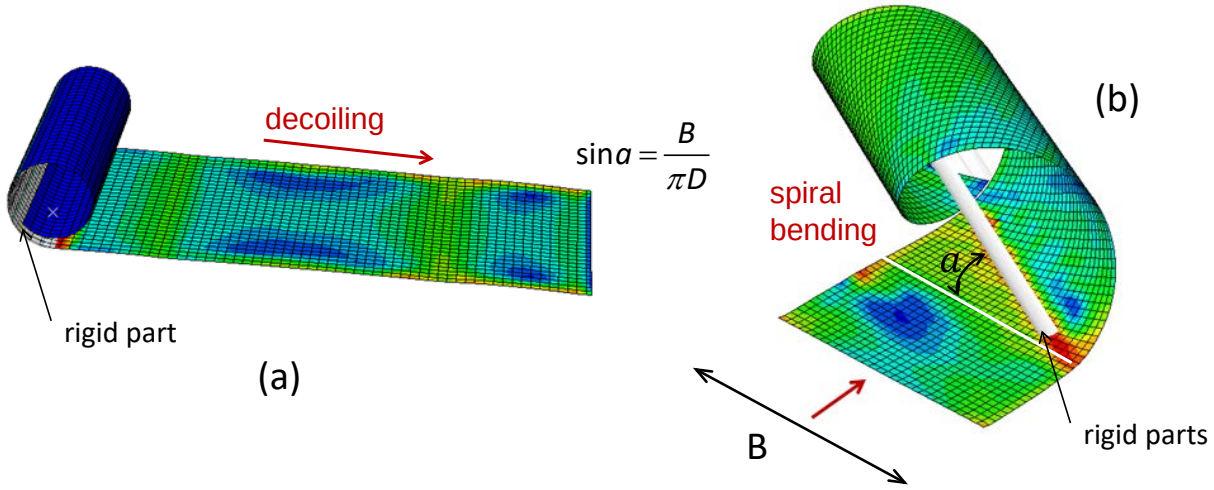

Figure 26: Finite element simulation of spiral pipe manufacturing (de-coiling and spiral bending) [42].

REFERENCES

[1] Karamanos, S. A., Sarvanis, G. C., Keil, B. and Card, R. J. (2017), "Analysis and Design of Buried Steel Water Pipelines in Seismic Areas.", ASCE *Journal of Pipeline Systems Engineering & Practice ,* Vol. 8, Issue 4.

[2] Moore, R. L. and Clark, J. W. (1952). "Torsion, compression, and bending tests of tubular sections machined from 75S-T6 rolled round rod", *National Advisory Committee for Aeronautics*, Washington, USA.

[3] Stephens, W. B., Starnes, J. H. and Almorth, B. O. (1975). Collapse of long cylindrical shells under combined bending and pressure loads. *AIAA J.* **13**, 20-25.

[4] Fabian, O. (1977). Collapse of cylindrical, elastic tubes under combined bending, pressure and axial loads. *Int'l J. Solids & Structures* **13**, 1257-1270.

[5] Mathon, C. and Limam, A. (2006). Experimental collapse of thin cylindrical shells submitted to internal pressure and pure bending. *Thin-Walled Structures* 44, 39-50.

[6] Stephens, W. B., Starnes Jr., J. H., and Almroth, B. O. (1975). *Collapse of Long Cylindrical Shells Under Combined Bending and Pressure Loads*, AIAA Journal, 13, 1, pp. 20-25.

[7] Emmerling, F. A. (1982). *Nichtlineare Biegung und Beulen von Zylindern und krummen Rohren bei Normaldruck* [in German], Ingenieur – Archiv, 52, pp. 1-16.

[8] Houliara, S. and Karamanos, S. A. (2006). Buckling and post-buckling of long pressurized elastic thin-walled tubes under in-plane bending. *Int'l J. Nonlinear Mechanics* 41, pp. 491-511.

[9] Bouwkamp, J. G. and Stephen, R. M. (1974). "Full-scale studies on the structural behavior of large diameter pipes under combined loading," *Structural Engineering Laboratory*, University of California, Berkeley.

[10] Sherman, D. R. (1976). "Tests of circular steel tubes in bending," *ASCE Journal of the Structural Division,* Vol. 102, no. ST11, pp. 2181-2195.

[11] Wilhoit, J. C. and Merwin, J. E. (1973). "Critical Plastic Buckling Parameters for Tubing in Bending Under Axial Tension," *Offshore Technology Conference*, Houston, USA.

[12] Tugcu, P. and Schroeder, J., (1979). "Plastic deformation and stability of pipes exposed to external couples," *Int. J. of Solids and Structures,* Vol. 15, pp. 643-658.

[13] Reddy, B. D. (1979). "An epxerimental study of the plastic buckling of circular cylinders in pure bending", *Int. J. of Solids and Structures,* Vol. 15, pp. 669-683.

[14] Kyriakides, S., and Ju, G.-T. (1992). "Bifurcation and localization instabilities in cylindrical shells under bending: Part I Experiments", *International Journal of Solids and Structures,* Vol. 29, pp. 1117-1142.

[15] Ju, G.-T., and Kyriakides, S. (1992). Bifurcation and localization instabilities in cylindrical shells under bending: Part II Predictions. *International Journal of Solids & Structures,* Vol. 29, pp. 1143-1171.

[16] Karamanos, S. A. and Tassoulas, J. L., (1996). "Tubular Members II: Local Buckling and Experimental Verification", ASCE *Journal of Engineering Mechanics*, Vol. 122, No. 1, pp. 72-78.

[17] Kyriakides, S. and Corona, E. (2007). *Mechanics of Offshore Pipelines: Volume 1: Buckling and Collapse*. Elsevier, Burlington, Massachusetts.

[18] Paquette, J. A. and Kyriakides, S. (2006). "Plastic buckling of tubes under combined axial compression and internal pressure", *International Journal of Mechanical Sciences,* Vol. 48, pp. 855-867.

[19] Gresnigt, A. M. (1986). "Plastic Design of Buried Steel Pipes in Settlement Areas", *HERON*, Vol. 31, No. 4, pp. 1-113.

[20] Van Foeken, R. J., and Gresnigt, A. M. (1998). “Effects of Buckling Deformations on the Burst Pressure of Pipes”, *Interim Report to AGA, TNO Bouw*, Rijswijk, The Netherlands.

[21] Mohareb, M. E., Alexander, S. D. B., Kulak, G. L. and Murray, D. W. (1993). "Laboratory testing of line pipe to determine deformational behavior", *12th International Conference on Offshore Mechanics and Arctic Engineering*, Glasgow, UK, Vol. 5, pp. 109-114.

[22] Yoosef-Ghodsi, N., Kulak, G. L., and Murray, D. W. (1995). "Some test results for wrinkling of girth-welded line pipe”, *14th International Conference on Offshore Mechanics and Arctic Engineering*, Copenhagen, Denmark, Vol. 5, pp. 379-387.

[23] Dorey, A. B., Murray, D. W., Cheng, J. J. R., Grondin, G. Y. and Zhou, Z. J. (1999). Testing and experimental results for NPS30 line pipe under combined loads. OMAE PL 99-5022, Proc. 18th *Int’l Conference on Offshore Mechanics and Arctic Engineering*, June 1999, St. Johns, Newfoundland.

[24] Dorey, A. B., Murray, D. W. and Cheng, J. J. R. (2000)."An experimental evaluation of critical buckling strain criteria", *International Pipeline Conference*, Calgary, Canada, pp. 71-80.

[25] Dorey, A. B., Murray D. W., Cheng, J. J. R. (2006), “Critical Buckling Strain Equations for Energy Pipelines - A Parametric Study”, *ASME Journal of Offshore Mechanics and Arctic Engineering*. Vol. 128, pp. 248-255.

[26] Pipeline Research Council International (2004), *Guidelines for the Seismic Design and Assessment of Natural Gas and Liquid Hydrocarbon Pipelines*, prepared by D. G. Honegger, and D. J. Nyman for the Pipeline Design, Construction & Operations Technical Committee of PRCI Inc., Houston, Texas.

[27] Suzuki, N., Kondo, J., Endo, S., Ishikawa, N., Okatsu, M., and Shimamura, J. (2007). “Strain capacity of X80 high-strain line pipes”. OMAE2007-29505, *26th International Conference on Offshore Mechanics and Arctic Engineering*, San Diego, CA.

[28] Limam, A., Lee, L.-H., Corona, E. and Kyriakides, S. (2010). “Inelastic wrinkling and collapse of tubes under combined bending and internal pressure”, *International Journal of Mechanical Sciences*, Vol. 52, pp. 637–647.

[29] Papadaki, C. I. (2015). “Ultimate Capacity of Gas Pipelines under Pressure and Bending”, *Diploma Thesis, Department of Mechanical Engineering, University of Thessaly*, Volos, Greece.

[30] Gresnigt, A. M. and Van Foeken, R. J. (2001). “Local Buckling of UOE and Seamless Steel Pipes,” in *International Offshore and Polar Engineering Conference (ISOPE)*, Stavanger, Norway.

[31] Zimmerman, T., Xie, J., Timms, C., and Asante, J. (2004). “Buckling resistance of large diameter spiral welded linepipe”, *International Pipeline Conference (IPC)*, Calgary, Canada.

[32] Spinelli, C. M., Demofonti, G., Fonzo, A., Lucci, A., Ferino, J., Di Biagio, M., Flaxa, V., Zimmermann, S., Kalwa, C., Knoop, F. M. (2011). “Full Scale Investigation on Strain Capacity of High Grade Large Diameter Pipes”, *3R International Journal*, Vol.1/2011, pp. 14-26.

[33] Ferino, J., Fonzo, A., Di Biagio, M., Demofonti, G., Spinelli, C. M., Karamanos, S. A. (2015), “Onshore pipeline high grade steel for challenge utilization.”, *International Journal of Offshore and Polar Engineering,* ISOPE, Vol. 25, No. 4, pp. 272–280.

[34] Zimmermann, S., Karbasian, H., and Knoop, F. M. (2013). "Helical Submerged Arc Welded Line Pipe Engineered For Strain Based Design", *Internalional Offshore and Polar Engineering (ISOPE)*, Anchorage, USA.

[35] Reinke, T., Sadowski, A. J., Ummenhofer, T. and Rotter, J. M. (2014). "Large Scale Bending Tests of Spiral Welded Steel Tubes,", *European Conference on Steel and Composite Structures*, Eurosteel 2014, Naples,.

[36] Van Es, S. H. J., Gresnigt, A. M., Vasilikis, D., and Karamanos, S. A. (2016), “Ultimate Bending Capacity of Spiral-Welded Steel Tubes - Part I: Experiments”, *Thin-Walled Structures*, Vol. 102, pp. 286-304.

[37] Vasilikis, D., Karamanos, S. A., Van Es, S. H. J. and Gresnigt, A. M. (2016), “Ultimate Bending Capacity of Spiral-Welded Steel Tubes - Part II: Predictions”, *Thin-Walled Structures*, Vol. 102, pp. 305-319.

[38] Peters, D. J., Broos, E. J., Van Es, S. H. J. and Gresnigt, A. M. (2015), “Local Buckling Resistance of Sand-filled Spirally Welded Tubes”, *25th International Ocean and Polar Engineering Conference,* Kona, Big Island, Hawaii, USA.

[39] Mecozzi, E., et al. (2017). “Strain-Based Design of Spiral-Welded Pipes for Demanding Pipeline Applications” SBD-SPIPE project, RFSR-CT-2013-00025, *Final Report to European Commission*, Brussels.

[40] Canadian Standard Association (2007), *Oil and Gas Pipeline Systems*, CSA-Z662, Mississauga, Ontario, Canada.

[41] Det Norske Veritas, (2010). *Submarine Pipeline Systems*, DNV-OS-F101 Standard, Oslo, Norway.

[42] Chatzopoulou, G., Sarvanis, G. C., Papadaki, C. I. and Karamanos, S. A., (2016), "The Effect of Spiral Cold-Bending Manufacturing Process on Pipeline Mechanical Behavior", IPC2016-64143, *Proceedings of the 11th International Pipeline Conference*, Calgary, Alberta, Canada.